

Synchronization of Microseismic Variations within a Minute Range of Periods

G. A. Sobolev, A. A. Lyubushin, Jr., and N. A. Zakrzhevskaya

*Schmidt Institute of Physics of the Earth, Russian Academy of Sciences (RAS),
Bol'shaya Gruzinskaya ul. 10, Moscow, 123995 Russia*

Received February 7, 2005

Abstract—Records obtained at the Petropavlovsk, Yuzhno-Sakhalinsk, Magadan, Yakutsk, and Obninsk IRIS broadband stations before the Kronotski (Kamchatka) earthquake are investigated with the use of various programs of processing and analysis of time series. Intervals of a stable manifestation of one or several periods of microseisms (synchronization intervals) inferred from data of different stations do not necessarily coincide in time. No anomalous meteorological effects are recorded in these intervals. Geodynamic phenomena on global and regional scales influence the duration and intensity of the synchronization intervals. As distinct from other stations, the Petropavlovsk record revealed asymmetric variations of the relaxation type that arose five days before the Kronotski earthquake and three days before the onset of intense foreshock activation. The amplitude of variations at this station exceeds the level of other stations by an order of magnitude, which indicates that the source of this earthquake was located in the Pacific seismically active region. The number of predominant periods at the Petropavlovsk station decreases toward the time moment of the Kronotski earthquake, and the poly-modal spectrum becomes unimodal, primarily due to the loss of shorter periods: a period of 37 min is most clearly expressed 1 h before the earthquake. The synchronization intervals of variations, as well as the foreshock activation, are indicators of the unstable state of a seismically active region.

INTRODUCTION

Numerous oscillating fields of various origins involving energy conversion act on the Earth in a very wide range of periods. For example, the energy of electromagnetic waves supplied to the Earth by external sources gives rise to elastic vibrations due to the piezoelectric effect and other thermodynamic coupling coefficients between these two types of energy, incoming heat induces elastic stresses in the Earth due to thermoelastic coupling coefficients, etc. The intensity of an external effect can be small compared to the forces acting in the Earth; however, the extent of their influence depends on the energy accumulated in rocks and cannot be interpreted in terms of linear effects.

The rhythms arising under the action of external or internal sources (i.e., the synchronization effect) have long been discussed by geophysicists. The influence of solar activity, earth tides, and climatic factors on seismicity is well known [Sytsinskii, 1963; Rykunov *et al.*, 1980; Rulev, 1991; Nikolaev and Nikolaev, 1993; Djadkov, 1997; Saltykov *et al.*, 1997; Tyupkin, 2002]. Stroboscopic and other techniques of detecting phase correlation are used to reveal the synchronization effect in relaxation processes if a series of observations involves well-pronounced events (earthquakes) playing the role of markers [Pykovsky *et al.*, 2003]. The synchronization of acoustic signals by electromagnetic pulses was established in laboratory experiments [Chelidze and Matcharashvili, 2003].

The question concerning the threshold of an external action that is sufficient for the synchronization of a process induced by substantially more powerful forces remains open. It is clear that an open energy system sensitive to a small external action must be in a metastable state [Sadovsky, 1989]. As the system approaches its instability, the threshold of an effective external action becomes lower. However, the Earth is permanently subjected to noise from natural and artificial sources. Therefore, the threshold of an effective detectable influence (including the trigger mechanism) apparently has a finite value exceeding the level of noise.

The effect of the appearance of hidden periodic variations in the flow of weak earthquakes and microseisms also belongs to the class of phenomena discussed [Sobolev, 2003, 2004]. In principle, these phenomena can be analyzed within the framework of the self-organized criticality (SOC) concept [Bak *et al.*, 1989; Sor-nette and Sammis, 1995], an important role in which is attached to the appearance of a remote correlation of seismic events (collective behavior). However, the physical mechanism of a possible remote correlation in seismology is not clear as yet; general theories of catastrophes and phase transitions in open energy systems need to be elaborated in relation to heterogeneous media.

Some of the issues considered in [Sobolev, 2004] require a more comprehensive analysis. Recall that the effect of hidden periodic microseismic variations in the range of periods of less than 1 h was investigated in the

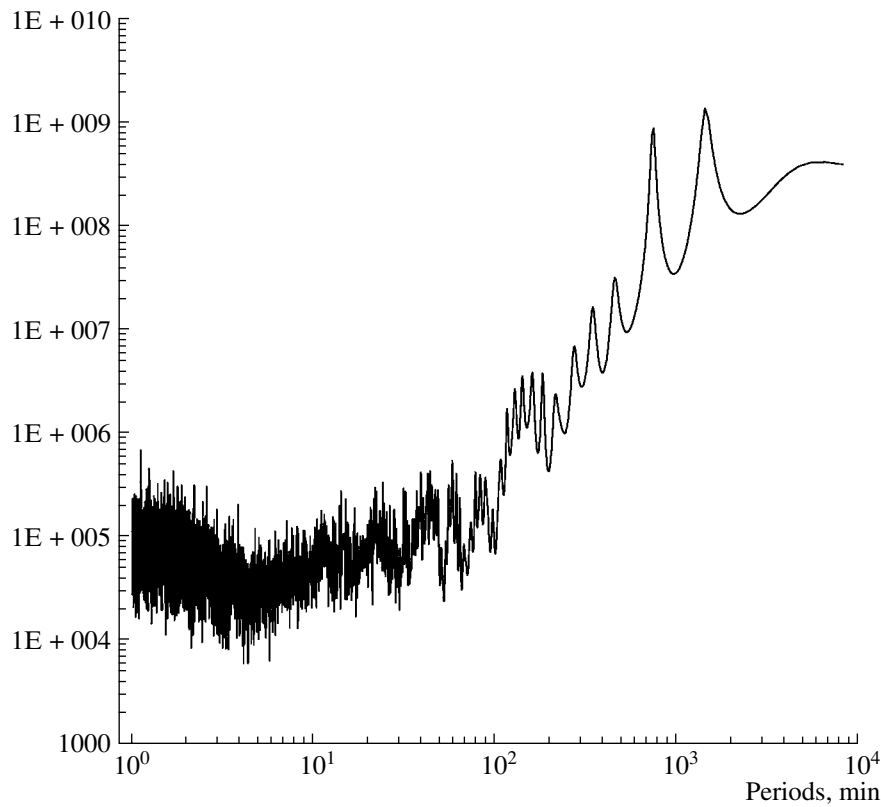


Fig. 1. Power spectrum of microseismic variations recorded at the Pet station from November 20, 1997, through December 5, 1997 (strictly up to the time moment of the Kronotski earthquake), calculated after 30-s discretization.

paper cited on the basis of data of a single seismic station, namely, the Petropavlovsk station on the Kamchatka Peninsula. Moreover, only one technique, proposed in [Lyubushin *et al.*, 1998], was used for the analysis of periodicity. Among others, important questions concerning the location of a synchronization region, as well as the structure and statistical properties of variations, remained open. These gaps are eliminated, to an extent, in the present investigation.

METHODS

As in [Sobolev, 2004], the most attention is given to the study of microseismic variations in the range of periods of less than 1 h. The power spectrum of variations calculated from 15-day data on the Z component obtained at the Petropavlovsk IRIS station on Kamchatka is shown in Fig. 1. The initial realization consisted of discrete measurements with a sampling rate of 20 Hz; however, before the estimation of the power spectrum, we passed to a discretization interval of 30 s (through averaging and thinning by a factor of 600). Three intervals of periods are noticeable in the plot of the spectrum. A decrease in the power of variations due to the gradually attenuating influence of microseisms of oceanic origin and weak earthquakes is observed in the range of short (up to 6 min) periods. The effect of earth

tides contributes to variations in the range of periods of hundreds of minutes, as is evident from the peaks at 1440 and 720 min corresponding to diurnal and semi-diurnal oscillations. The IRIS station response to tides was probably due to tilts of the pedestal. The range of tens of minutes is largely free of the above effects and is poorly studied. This range includes overtones of free oscillations of the Earth [Zharkov and Trubitsyn, 1980] and was examined episodically, after strong earthquakes. The frequency range and comprehensive meteorological measurements at IRIS stations favor a detailed analysis of variations in this range, including variations preceding strong seismic events.

Analysis of Hidden Periodicities in Sequences of Peak Values at a Given Level

The method used here was proposed in [Lyubushin *et al.*, 1998] and is intended for the identification of periodic components in a sequence of events. Let

$$t_i, \quad i = 1, \dots, N \quad (1)$$

be the times of sequential events observed in the interval $(0, T]$. We consider the following model of the intensity, containing a periodic component:

$$\lambda(t) = \mu(1 + a \cos(\omega t + \varphi)), \quad (2)$$

where the frequency ω , the amplitude a ($0 \leq a \leq 1$), the phase angle φ ($\varphi \in [0, 2\pi]$), and the multiplier $\mu \geq 0$ (describing the Poissonian part of the intensity) are parameters of the model. Thus, the Poissonian part of the intensity is modulated by a harmonic oscillation.

At a fixed frequency ω , the logarithmic function of likelihood [Cox and Lewis, 1966] for the series of observed events is

$$\begin{aligned} \ln L(\mu, a, \varphi | \omega) &= \sum_{t_i} \ln(\lambda(t_i)) - \int_0^T \lambda(s) ds \\ &= N \ln(\mu) + \sum_{t_i} \ln(1 + a \cos(\omega t_i + \varphi)) \\ &\quad - \mu T - \frac{\mu a}{\omega} [\sin(\omega T + \varphi) - \sin(\varphi)]. \end{aligned} \quad (3)$$

Maximizing (3) with respect to the parameter μ , we easily find

$$\begin{aligned} \mu &= \hat{\mu}(a, \varphi | \omega) \\ &= \frac{N}{T + a(\sin(\omega T + \varphi) - \sin(\varphi)) / \omega}. \end{aligned} \quad (4)$$

Substituting (4) into formula (3), we obtain

$$\begin{aligned} &\ln(L(\hat{\mu}, a, \varphi | \omega)) \\ &= \sum_{t_i} \ln(1 + a \cos(\omega t_i + \varphi)) + N \ln(\hat{\mu}(a, \varphi | \omega)) - N. \end{aligned} \quad (5)$$

We should note that the expression $\hat{\mu}(a = 0, \varphi | \omega) \equiv \hat{\mu}_0 = N/T$ is an estimate of the intensity of the process provided that it is a homogeneous Poissonian process (of the purely random type).

Thus, the increment of the logarithmic likelihood function in the intensity model incorporating a harmonic component of a given frequency ω superimposed on a purely random flow of events amounts to

$$\begin{aligned} &\Delta \ln L(a, \varphi | \omega) \\ &= \sum_{t_i \in} \ln(1 + a \cos(\omega t_i + \varphi)) + N \ln(\hat{\mu}(a, \varphi | \omega) / \hat{\mu}_0). \end{aligned} \quad (6)$$

We set

$$\begin{aligned} R(\omega) &= \max_{a, \varphi} \Delta \ln L(a, \varphi | \omega), \\ 0 \leq a \leq 1, \quad \varphi &\in [0, 2\pi]. \end{aligned} \quad (7)$$

Function (7) can be regarded as a generalization of the spectrum of a sequence of events. The plot of this function shows to what extent the periodic intensity model is more advantageous compared to the purely random model. The maximum values of function (7) specify frequencies that are present in the flow of events.

The calculation of function (7) using observation time moments not in the entire interval $(0, T]$ but inside a moving window of a given width T_w is the next obvious generalization of the model. Let τ be the time of the right-hand end of the moving window. Then expression (7) becomes a function of two arguments, $R(\omega, \tau | T_w)$, which can be visualized in the form of 2-D maps or 3-D images on the plane of arguments (ω, τ) . This frequency–time diagram makes it possible to trace the evolution of periodic components inside the flow of events under consideration [Lyubushin, 2002; Sobolev, 2003].

Wavelet Analysis of Seismograms

This analysis is effective for investigating the frequency–time dynamics of a nonstationary series of observations consisting, for example, of pulses of different amplitudes and duration. Since the use of such analysis in seismology and geophysics is still very limited, we describe in greater detail the method applied here.

The orthogonal multiresolution analysis (the wavelet expansion) of a signal $x(s)$ as a function of a continuous argument s is defined by the formula [Daubechies, 1992; Mallat, 1998]

$$\begin{aligned} x(s) &= \sum_{\alpha=-\infty}^{+\infty} x^{(\alpha)}(s), \\ x^{(\alpha)}(s) &= \sum_{j=-\infty}^{+\infty} b^{(\alpha)}(\tau_j^{(\alpha)}) \psi^{(\alpha)}(s - \tau_j^{(\alpha)}), \\ \tau_j^{(\alpha)} &= j2^\alpha. \end{aligned} \quad (8)$$

Here, α is the number of the detail level;

$$b_j^{(\alpha)} = b^{(\alpha)}(\tau_j^{(\alpha)}) = \int_{-\infty}^{+\infty} x(s) \psi^{(\alpha)}(s - \tau_j^{(\alpha)}) ds \quad (9)$$

are the wavelet coefficients at the α th detail level corresponding to the time moment $\tau_j^{(\alpha)}$; and $\psi^{(\alpha)}(s)$ are the basis functions of the α th level, which are obtained by extension and translation of the mother wavelet function $\Psi(s)$:

$$\begin{aligned} \psi^{(\alpha)}(s) &= (\sqrt{2})^{-\alpha} \Psi(2^{-\alpha} s), \\ \psi^{(\alpha)}(s - \tau_j^{(\alpha)}) &= (\sqrt{2})^{-\alpha} \Psi(2^{-\alpha} s - j). \end{aligned} \quad (10)$$

The function $\Psi(s)$ is constructed under the following conditions: it should be compactly supported and have a unit norm in $L_2(-\infty, +\infty)$, and an infinite set of functions $\psi^{(\alpha)}(s - \tau_j^{(\alpha)})$ that are copies of the mother function translated to the points $\tau_j^{(\alpha)}$ and stretched (or con-

tracted) by a factor of 2^α should form an orthonormal basis in $L_2(-\infty, +\infty)$. For example, if

$$\Psi(s) = -1 \text{ for } s \in \left(0, \frac{1}{2}\right] \tag{11}$$

$$+1 \text{ for } s \in \left(\frac{1}{2}, 1\right] \text{ and zero for other } t,$$

formula (8) provides the expansion of the function $x(s)$ in Haar wavelets. Function (11) is the simplest and most compact orthogonal finite wavelet. The Daubechies functions $\Psi(s) = D_{2p}(s)$ of the order $2p$, possessing the properties

$$D_{2p}(s) = 0 \text{ outside the interval } [-p + 1, p], \tag{12a}$$

$$\int_{-\infty}^{+\infty} s^k D_{2p}(s) ds = 0 \text{ for } k = 0, \dots, (p - 1), \tag{12b}$$

form the most widely used family of orthogonal wavelet functions.

With an increase in the number p of vanishing moments in formula (12b), the function $D_{2p}(s)$ becomes smoother, although the number of its continuous derivatives is not proportional to the parameter p . For example, the Daubechies function of the 4th order $D_4(s)$ sets to zero the zeroth and first moments and is continuously differentiable at all points except a countable set of points of the form $k2^{-l}$, where k and l are whole numbers. At such points, $D_4(s)$ has a left-hand derivative and does not have a right-hand derivative. Note that Haar wavelet (4) is a second-order Daubechies wavelet ($p = 1$). We used a dictionary of 17 wavelets: 10 ordinary orthogonal Daubechies wavelets of orders from 2 to 20 (the use of higher orders entails numerical instability) and 7 so-called ‘‘symlets,’’ which are Daubechies wavelets whose basis functions are more symmetric compared to ordinary wavelets [Chui, 1992; Daubechies, 1992; Mallat, 1998]. Symlets possess the same properties of compactness, orthogonality, completeness, and smoothness as wavelets (12); however, for orders of 2 to 6, they coincide with the ordinary orthogonal Daubechies basis, while, for orders of 8 to 20, some distinctions appear in the form of the basis function. As a consequence, the total number of variants of orthogonal compact basis functions used here is 17.

Now, we address the situation when $z(t)$ is a signal discrete in time t having a length of N measured values, $t = 1, \dots, N$. We assume that N is an integer of the form 2^m because this is convenient for the subsequent application of the fast wavelet transform. If N is not equal to 2^m , the signal $z(t)$ is complemented by zeros to make it 2^m long, where m is the minimum integer such that $N \leq 2^m$.

The formula of the multiple-resolution analysis in the case of a finite sample and discrete time is

$$z(t) = a_1^{(m)} + \sum_{\beta=1}^m z^{(\beta)}(t),$$

$$z^{(\beta)}(t) = \sum_{j=1}^{2^{(m-\beta)}} c^{(\beta)}(\tau_j^{(\beta)}) \Psi^{(\beta)}(t - \tau_j^{(\beta)}), \tag{13}$$

$$\tau_j^{(\beta)} = j2^\beta,$$

where $z^{(\beta)}(t)$ is the component of the signal belonging to the detail level of the number β and $a_1^{(m)}$ is a constant proportional to the mean of the sample [Chui, 1992; Daubechies, 1992; Mallat, 1998; Press *et al.*, 1996]. The coefficients $c_j^{(\beta)} = c^{(\beta)}(\tau_j^{(\beta)})$ in (13) can be represented, similarly to formula (9), as the convolution of the basis function $\Psi^{(\beta)}(s)$ of the continuous argument s with a certain signal $\tilde{z}(s)$:

$$c_j^{(\beta)} = \int_{-\infty}^{+\infty} \tilde{z}(s) \Psi^{(\beta)}(s - \tau_j^{(\beta)}) ds. \tag{14}$$

The signal $\tilde{z}(s)$ is obtained from the signal $z(t)$ with the discrete time t through the interpolation formula

$$\tilde{z}(s) = \sum_t z(t) \Phi(s - t), \tag{15}$$

where the function $\Phi(s)$ is called the *scaling* function of the wavelet expansion. For example, in the case of Haar wavelet (11), $\Phi(s) = 1$ if $s \in [0, 1]$, and $\Phi(s) = 0$ for all other s ; consequently, the interpolated signal will be a piecewise-continuous function. In the general case of orthogonal Daubechies wavelets, the scaling function is orthogonal to the principal basis function $\Psi(s)$, $\int_{-\infty}^{+\infty} \Psi(s) \Phi(s) ds = 0$, and has the same properties of smoothness and a compact carrier of the same length as $\Psi(s)$ (but not coinciding with it completely): $\Phi(s) = 0$ outside the interval $[0, 2p - 1]$.

If the discrete signal $z(t)$ is obtained from a signal continuous in time $x(s)$ that is measured at a time step Δs , then, if $\Delta s \rightarrow 0$, the interpolated signal $\tilde{z}(s)$ always tends in the mean-square metric L_2 to the initial signal $x(s)$. If the scaling function $\Phi(s)$ corresponding to the Daubechies basis of the order $2p$ is used in formula (15), the interpolated signal $\tilde{z}(s)$ will have $p - 1$ first derivatives continuous almost everywhere, with the possible exception of a countable set of points, regardless of the smoothness of the initial signal $x(s)$. However, if $\Delta s \rightarrow 0$, these derivatives will tend in the integral metric L_2 to the derivatives of the initial signal only if $x(s)$ is differentiable almost everywhere also $p - 1$ times.

Thus, the choice of the wavelet for the signal analysis must correspond to its smoothness.

Regardless of the possible origin of the signal $z(t)$ obtained by the discretization of the continuous signal $x(s)$ with a certain time step Δs , the coefficients c_j^β of discrete expansion (13) are a result of the application of a successive linear filtering of the discrete signal. At the first step, the discrete signal is split into two parts: the wavelet coefficients of the first detail level $c_j^{(1)}$ (or the “detail signal” of the first level) and the so-called approximating (smoothed) signal $a_j^{(1)}$, using the formula

$$\begin{aligned} c_j^{(1)} &= \sum_t g(t-2j)a_t^{(0)}, \\ a_j^{(1)} &= \sum_t h(t-2j)a_t^{(0)}, \\ a_t^{(0)} &\equiv z(t), \quad j = 1, \dots, N/2. \end{aligned} \tag{16}$$

The coefficients of the linear filter $g(k)$ in (16) possess the property of detecting high frequencies, and the coefficients $h(k)$ possess the property of smoothing. Note that formulas (16) involve not only the linear filtration but also a twofold downsampling procedure; therefore, the detail and approximating signals contain half as many samples as the initial signal. Because of a finite length of the sample, technical difficulties are associated with the application of formulas (16) to the beginning and the end of the sample. These difficulties can be overcome by various methods such as, for example, the consideration of the sample $z(t)$ on a ring rather than in an interval. In this case, edge distortions of the wavelet filtering results similar to those produced by the cyclic effect of the discrete Fourier transform [Press *et al.*, 1996] can arise. Step (16) is repeated $m - 1$ times (recall that $N = 2^m$):

$$\begin{aligned} c_j^{(\beta+1)} &= \sum_t g(t-2j)a_t^{(\beta)}, \\ a_j^{(\beta+1)} &= \sum_t h(t-2j)a_t^{(\beta)}, \\ j &= 1, \dots, N2^{-(\beta+1)}. \end{aligned} \tag{17}$$

According to formula (17), at each new detail level of the wavelet expansion, the approximating signal $a_j^{(\beta)}$ of the preceding detail level is split into its high-frequency component $c_j^{(\beta+1)}$ and the progressively more smoothed signal $a_j^{(\beta+1)}$. The number of components in the detail signal (i.e., the number of wavelet coefficients) and in the smoothed (approximating) signal decreases by two times as the number of the detail level

increases by unity. The coefficient $a_1^{(m)}$ in (13) is the approximating “signal” corresponding to the deepest smoothing at the final detail level m . The coefficients $g(k)$ and $h(k)$ of the linear filters (called the conjugated mirror filters) are interrelated as $g(k) = (-1)^{1-k}h(1-k)$ in accordance with the scaling equations of the orthogonal multiple-resolution analysis

$$\begin{aligned} \frac{1}{\sqrt{2}}\Phi(t/2) &= \sum_{k=-\infty}^{+\infty} h(k)\Phi(t-k), \\ \frac{1}{\sqrt{2}}\Psi(t/2) &= \sum_{k=-\infty}^{+\infty} g(k)\Phi(t-k) \end{aligned} \tag{18}$$

for the scaling and mother basis functions. For the Daubechies finite basis functions $D_{2p}(s)$, the number of nonvanishing coefficients in the linear mirror filters $g(k)$ and $h(k)$ is equal to the order of the function $2p$. For example, for the Haar wavelet, $h(k) = 1/\sqrt{2}$ for $k = 0, 1$ and $h(k) = 0$ for all other k . For the Daubechies functions of orders 4 and 6, the coefficients of mirror filters are determined analytically from linear equations following from condition (12b), nullifying a given number of first moments; however, for higher orders, these linear equations are solved numerically. We should note that, as the wavelet order increases, the conditioning of the linear equations deteriorates and the roundoff error increases. Therefore, calculations are usually restricted to wavelets of an order not exceeding 20.

Algorithmically, the wavelet transform is a linear orthogonal transform of the N -dimensional vector of a sample $z(t)$ into the vector of coefficients $C_z^{(N)} = (a_1^{(m)}, c_1^{(m)}, \dots, (c_j^{(\beta)}, j = 1, \dots, n_\beta), \dots)$, whose length is also equal to N . The vector $C_z^{(N)}$ consists of the constant $a_1^{(m)}$ as a first component and the successively arranged coefficients of all detail levels, beginning from the m th, $(m - 1)$ th, and so on, up to the coefficients of the first detail level, which occupy the entire second half of the vector [Press *et al.*, 1996]. The inverse transformation of the vector $C_z^{(N)}$ yields the initial sample $z(t)$. Note that the inverse wavelet transformation is also effected in the form of consecutive steps reconstructing the approximating signal of the level β from the wavelet coefficients $c_k^{(\beta+1)}$ and the approximating signal $a_k^{(\beta+1)}$ of the level $(\beta + 1)$ with the use of mirror-conjugated filters by the formula

$$\begin{aligned} a_j^{(\beta)} &= \sum_k h(j-2k)a_k^{(\beta+1)} \\ &+ \sum_k g(j-2k)c_k^{(\beta+1)}, \quad j = 1, \dots, N2^{-\beta}. \end{aligned} \tag{19}$$

The inverse transformation starts with the coefficients $a_1^{(m)}$ and $c_1^{(m)}$ of the final (lowest-frequency) detail level of the number m and ends at the first level. In this case, the number of components in the approximating signal doubles each time, when the number of the detail level decreases until the sequence of reconstructions stops at the first detail level and the number of components becomes equal to N . The forward and inverse wavelet transforms (17) and (19) can be numerically implemented in the form of fast algorithms requiring $O(N)$ operations and a shorter computation time compared to the fast Fourier transform [Chui, 1992; Daubechies, 1992; Mallat, 1998; Press *et al.*, 1996]. The component $z^{(\beta)}(t)$ is a result of the inverse transformation of the vector of coefficients of the $C_z^{(N)}$ type provided that all coefficients, except those corresponding to the level β , are set at zero.

At a sufficiently large value of N , the component $z^{(\beta)}(t)$ is localized within the frequency band

$$[\Omega_{\min}^{(\beta)}, \Omega_{\max}^{(\beta)}] = [1/(2^{(\beta+1)}\Delta s), 1/(2^\beta\Delta s)], \quad (20)$$

where Δs is the length of the sampling interval. The value of the coefficient $c_j^{(\beta)}$ reflects the behavior of the signal $z(t)$ in the vicinity of the point $\tau_j^{(\beta)}$ in the interval of a length equal to $p2^\beta$ values. Consequently, the smoother the wavelet, the wider this interval. However, the main variations (bursts) in the finite basis function $\psi^{(\beta)}(s)$ are always concentrated in the interval 2^β long, regardless of the smoothness parameter p . Therefore, we associate each coefficient $c_j^{(\beta)}$ with “a temporal zone of responsibility” of length $\Delta T^{(\beta)} = \Delta s 2^\beta$. The product of the width $\Delta\Omega^{(\beta)} = 1/(2^{\beta+1}\Delta s)$ of frequency range (20) by the length of the time interval $\Delta T^{(\beta)}$ gives the area of the so-called “Heisenberg box” on the frequency–time plane; this area is equal to $1/2$, regardless of the detail level under consideration.

The smallest scale detail level in formula (13) is the first level, and the total number of detail levels m depends on the sample length. The values $c_j^{(\beta)}$ and $a_1^{(m)}$ are calculated by using the fast wavelet transform [Daubechies, 1992; Mallat, 1998; Press *et al.*, 1996]. These values uniquely determine the initial sample $z(t)$, which can be reconstructed from given values of $c_j^{(\beta)}$

and $a_1^{(m)}$ by the inverse fast wavelet transform. The detail level can be associated with the number of the frequency (the frequency discrete) in the classical discrete Fourier transform. The wavelet expansion differs from the Fourier analysis by a substantially rarer (uniform on the logarithmic scale) set of “wavelet frequencies.” This is the price for such an important property as the compactness of basis functions, which is absent in the Fourier expansion and allows one to locate short-

lived anomalies (bursts) much more accurately. Moreover, the compactness of basis functions makes the wavelet analysis applicable to nonstationary and non-Gaussian time series, the Fourier analysis of which, although formally possible, is inefficient.

Although the ordinary wavelet expansion possesses such a useful property as a high-accuracy localization in time of nonstationary signals, the reverse side of this property is a poor resolution in frequency, in accordance with the Heisenberg principle. The wavelet-packet expansion partially eliminates this drawback at the expense of a certain decrease in the time resolution. The realization of the packet splitting is based on the hierarchical scheme of successive wavelet transforms of the initial coefficients $c_j^{(\beta)}$. The orthogonal wavelet-packet expansion of the signal can be, by analogy with formula (13), written as the sum

$$z(t) = a_1^{(m)} + \sum_{\beta = m_q + 1}^m z^{(\beta)}(t) + \sum_{\beta = 1}^{m_q} \sum_{\gamma = 1}^q z^{(\beta, \gamma)}(t). \quad (21)$$

The quantity q can be equal to 2, 4, 8, ..., i.e., $q = 2^r$ ($r = 1, 2, 3, \dots$), and it controls the number of sublevels into which an ordinary detail level is split. For a given value of q , the maximum number $m_q < m$ of the detail level β that can be split is determined from the condition that this level must contain at least q wavelet coefficients. The components $z^{(\beta, \gamma)}(t)$ are frequency-ordered and split frequency band (20) of detail level β into q equal parts. Thus, the signal $z^{(\beta, \gamma)}(t)$ is localized in frequency within this band:

$$[\Omega_{\min}^{(\beta, \gamma)}, \Omega_{\max}^{(\beta, \gamma)}], \quad \Omega_{\min}^{(\beta, \gamma)} = \Omega_{\min}^{(\beta)} + (\gamma - 1)\Delta\Omega^{(\beta)},$$

$$\gamma = 1, \dots, q; \quad (22)$$

$$\Omega_{\max}^{(\beta, \gamma)} = \Omega_{\min}^{(\beta, \gamma)} + \Delta\Omega^{(\beta)}, \quad \Delta\Omega^{(\beta)} = (\Omega_{\max}^{(\beta)} - \Omega_{\min}^{(\beta)})/q.$$

If n_β ordinary wavelet coefficients correspond to the detail level with the number β , n_β/q wavelet-packet coefficients $c_j^{(\beta, \gamma)}$, $j = 1, \dots, n_\beta/q$ correspond to each sublevel γ of the packet expansion. The Heisenberg boxes for these coefficients have a time length q times larger compared to the initial coefficients $c_j^{(\beta)}$, but their frequency side is q times smaller (consequently, the area of the Heisenberg boxes remains unchanged and equal to $1/2$).

To obtain the component $z^{(\beta, \gamma)}(t)$, it is necessary to perform successive inverse wavelet transformations starting with the coefficients $c_j^{(\beta, \gamma)}$. The final inverse transformation is applied to a certain set of coefficients $w_j^{(\beta, \gamma)}$, $j = 1, \dots, n_\beta$ that occupy in an analogue of the vector $C_z^{(\beta)}$ the same positions as the ordinary coefficients $c_j^{(\beta)}$ of the expansion of the signal $z(t)$. However,

the inverse transformation with these coefficients yields the component $z^{(\beta, \gamma)}(t)$ rather than $z^{(\beta)}(t)$. The coefficients $w_j^{(\beta, \gamma)}$ are called modified wavelet-packet coefficients of the signal $z(t)$. Thus, the modified coefficients $w_j^{(\beta, \gamma)}$ are the ordinary wavelet coefficients at the detail level β for the case when only the component $z^{(\beta, \gamma)}(t)$ of the initial signal rather than the signal itself is fed to the input of the forward transformation. The Heisenberg boxes for the coefficients $w_j^{(\beta, \gamma)}$ have the same time length as for $c_j^{(\beta)}$; however, their frequency length is equal to that of the coefficients $c_j^{(\beta, \gamma)}$. Thus, the transition from the ordinary wavelet-packet coefficients $c_j^{(\beta, \gamma)}$ to the modified coefficients $w_j^{(\beta, \gamma)}$ is a procedure narrowing the uncertainty time interval (decreasing the time length of the Heisenberg box). Note that such a transition preserves the energy of the expansion coefficients: $\sum_{j=1}^{n_\beta} (w_j^{(\beta, \gamma)})^2 = \sum_{j=1}^{n_\beta/q} (c_j^{(\beta, \gamma)})^2$.

If a two-dimensional map consisting of the frequency-ordered Heisenberg boxes of the modified coefficients $w_j^{(\beta, \gamma)}$ is constructed in the time–frequency plane and each box is painted in accordance with a palette proportional to the absolute values of the wavelet-packet coefficients $w_j^{(\beta, \gamma)}$ (or to their logarithms), we will obtain a diagram visualizing the temporal behavior of the main time scales (or periods) of a nonstationary signal. In its outward appearance, this mosaic of wavelet-package Heisenberg boxes may be inferior in aesthetic perception, for example, to the traditional spectral–temporal diagrams. However, it provides a more accurate and adequate idea of the frequency–time dynamics of an essentially nonstationary signal consisting of a set of short-lived bursts of various scales that can differ significantly in shape from a harmonic oscillation.

RESULTS

Figure 2 demonstrates the spectral–temporal diagrams of the increment in the logarithmic likelihood function $\Delta \ln L$ obtained from data of the following five IRIS seismic stations with similar characteristics: Petropavlovsk (Pet) (53.024°N, 158.653°E), Yakutsk (Yak) (62.031°N, 129.681° E), Obninsk (Obn) (55.114°N, 36.569°E), Magadan (Mag) (59.575°N, 150.768°E), and Yuzhno-Sakhalinsk (Yss) (46.954°N, 142.755°E). The Pet, Yak, and Obn stations are widely separated in longitude and are located in areas with different seismogeological conditions. The Pet station is located in a highly active seismic zone on the Pacific coast; the Yak station is located in a weakly active region of the East Siberian platform; and the Obn station is located on the seismically passive East European

platform. The Mag and Yss stations are located, respectively, at the northern and southern boundaries of the Sea of Okhotsk, characterized by the occurrence of deep earthquakes.

The dark bands in the diagrams of Fig. 2 indicate the presence of periodic variations in the range of periods from 20 to 60 min. The increment $\Delta \ln L$ was estimated for the sequence of time moments corresponding to the maximums in seismograms exceeding the level equal to the window-averaged value plus the sample estimate of the standard deviation in the same window. The time is measured from 00:00 Greenwich time (UTC) of December 2, 1997. Values of $\Delta \ln L$ were calculated in a time window of the width $\Delta T = 3$ h with the step $\Delta S = 1$ h, so that the diagrams in the figure are presented from 03:00 UTC of December 2. The final points on the time scale of the diagrams (83 h) correspond to 11:00 UTC of December 5; i.e., they were obtained 27 min before the Kronotski (Kamchatka) earthquake with the magnitude 7.7. The Pet, Mag, Yss, Yak, and Obn stations are located at respective distances of 310, 900, 2360, 3750, and 8060 km from its epicenter (54.64° N, 162.55° E).

The beginning of the analyzed period was chosen considering that December 2, 1997, was characterized by a quiet seismic situation in the areas of the stations, where, according to data of the RAS Geophysical Service, no local earthquakes of the energy class $K > 10$ were observed. Four remote earthquakes (off the Alaska coast, $M_s = 5.2$; on the Mid-Atlantic Ridge, $M_s = 4.1$; in the Philippines, $M_w = 5.3$; and in the Mediterranean Sea, $M_s = 4.3$) noted in the ISC catalog represent a common phenomenon.

The seismic process in the epicentral area of the future Kronotski earthquake was dramatically activated on Kamchatka in the middle of the day on December 3. Three earthquakes with $K > 10$ and three earthquakes with $K > 11$ occurred during this day. The onset of the foreshock process is marked by the arrow labeled F in the upper diagram of Fig. 2. According to the catalog of the Kamchatka Experimental–Methodological Seismic Party (KEMSP), the activation continued during the next day, when the number of shocks increased. Seven events with $K > 10$, five with $K > 11$, and one with $K = 12.8$ (at 22:41:48 UTC) were recorded on December 4. The last event is marked by the arrow labeled F_a in Fig. 2. On the day of the Kronotski earthquake (December 5), 13 foreshocks with $K > 10$, 12 with $K > 11$, and 4 with $K > 12$, including a foreshock with $K = 12.5$ (08:08:47 UTC) were recorded before the time moment of this earthquake. The last foreshock is marked in Fig. 2 by the arrow labeled F_b. Altogether, the foreshock series included 100 earthquakes of classes $K > 8.5$. As is evident from Fig. 2, the first series of periodic microseismic variations arose at all of the five stations at the end of December 2 to the beginning of December 3 (Greenwich time). The second series started at about 22:00 UTC of December 4 (71 h in the diagrams) and contin-

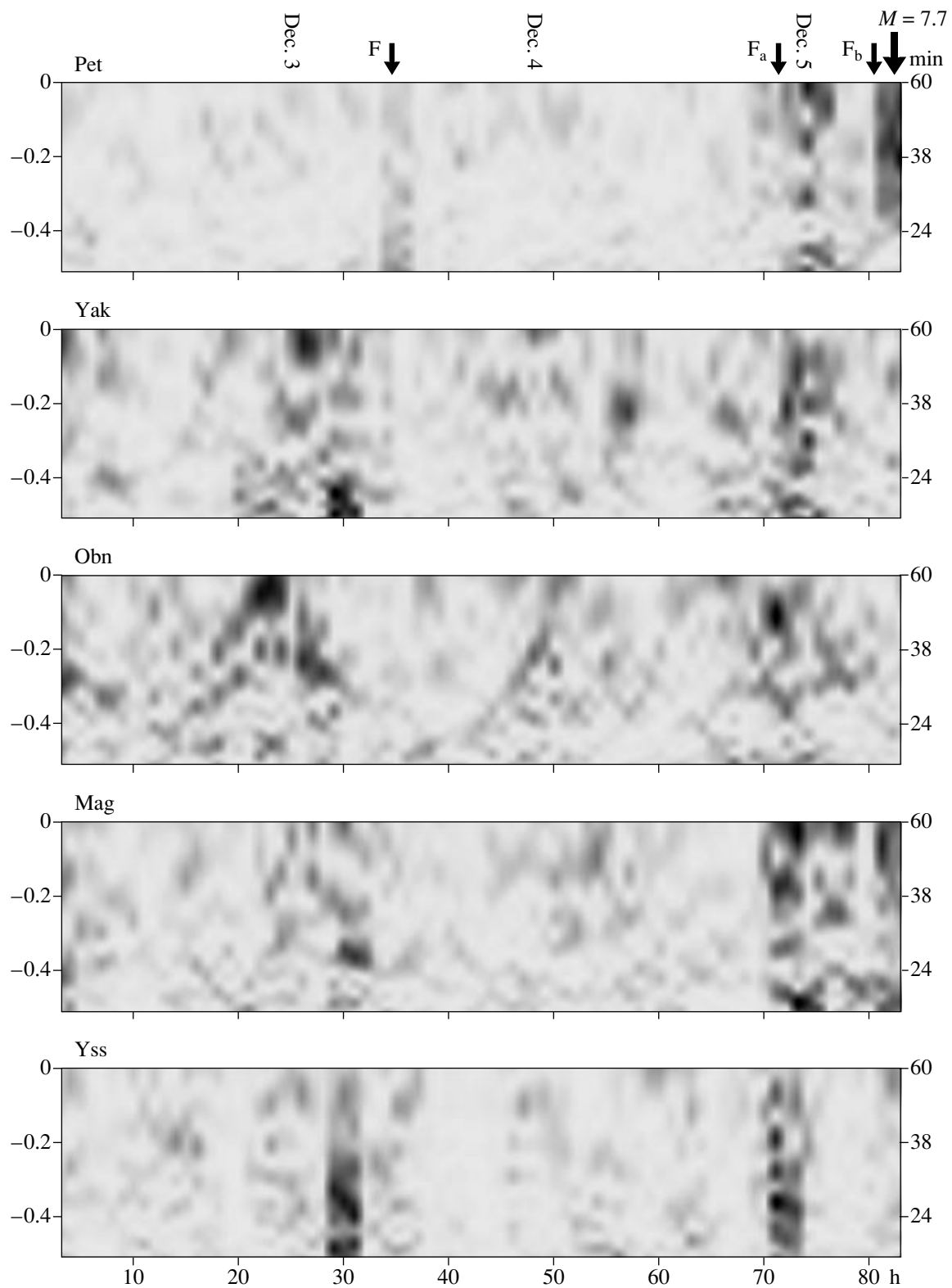


Fig. 2. Spectral time diagrams of the increment of the logarithmic likelihood function $\Delta \ln L$ for the microseisms recorded at the Pet, Yak, Obn, Mag, and Yss stations. The ordinates show the spectral period (to the right) and its logarithm (to the left). The thick arrow marks the time moment of the Kronotski ($M = 7.7$) earthquake of December 5, 1997. The arrows labeled F, F_a , and F_b mark the onset of foreshock activation and the two strongest foreshocks.

ued up to the time moment of the main shock of the Kronotski earthquake (83 h).

The first series of shocks was characterized by the following features. The variations were not synchronous at different stations. The earliest shocks of December 2 were recorded at the Obn station, located at the greatest distance to the west of Kamchatka. These variations end in the Obn diagram after 29 h. Approximately at this time, the most pronounced variations are noted at the Yak, Mag, and Yss stations. They disappear after 31 h. One should bear in mind that, with the window shift $\Delta S = 1$ h, the visible width of the dark band in Fig. 1 does not mean that the periodic variations of interest continued for 3 h. They could have had a shorter duration, but it must have been sufficient for detecting these variations by the program used for calculating the function $\Delta \ln L$. The following characteristic feature is revealed in the diagram of the Pet station: periodic variations appear with a delay of 4–5 h relative to the Yak, Mag, and Yss stations and coincide in the onset time with the foreshock activation of the Kronotski earthquake.

During the second series of periodic variations, the Pet diagram displays two features distinguishing it from the diagrams of the other stations. First, the best expressed maximums appear in the diagram about 2 h after the maximums at the Obn, Mag, and Yss stations. Second, 3 h before the Kronotski earthquake, the periodic variations are most distinct at the Pet station. Their presence at the Mag station is possibly connected with the fact that the Mag station is relatively close to both the earthquake epicenter (900 km) and the Pet station (1140 km). Supposing that the maximums are due to elastic vibrations in the Earth and taking into account that their periods range from 20 to 60 min, the wavelength λ is about 10000 km, so that the distance between the Pet and Mag stations is $<1/4\lambda$.

A conspicuous feature of the second series of the $\Delta \ln L$ maximums is that the maximum with a period of ~ 37 min, which arose 3 h before the earthquake, is present only at the Pet station.

As was noted in [Sobolev, 2004], periodic variations in a range of periods shorter than 1 h arose before the Kronotski earthquake after its foreshocks. In this connection, we analyzed in detail the structure of records in the period of the strongest foreshocks F_a and F_b , which occurred 13 and 3 h before the main shock (70.5 and 80.5 h in the diagram of the Pet station in Fig. 2). This analysis was based on data of the Pet and Yak stations, taking into consideration that variations after the foreshock F_a arose at both stations, whereas variations after the foreshock F_b were recorded only at the Pet station.

A 3-h interval of the Z-component record obtained at the Pet station including the foreshock F_a and a weaker preceding foreshock is presented in the upper panel of Fig. 3a. The number of 20-Hz discretized values is shown on the abscissa axis. As noted above, the

window $\Delta T = 3$ h was used for the identification of the periodic variations shown in Fig. 2. The structure of variations obtained after averaging of the initial record over 1200 discretization points (i.e., after the reduction to 1-min values) is demonstrated in the two lower panels of Fig. 3a. Plots 2 and 3 are obtained after the application of low-frequency filters rejecting high frequencies beginning from the periods 5 and 20 min, respectively. All three plots are synchronized in time. This figure shows that variations in the range of periods <1 h took place both before and after the foreshock, and no substantial distortions of their structures are observed immediately after the foreshock. The calculation of periodograms of the curves in the range of interest revealed maximums at 61.3 and 18.4 min. As follows from comparison of the upper and the two lower curves of Fig. 3a, the amplitude of variations in the range of periods <1 h is 20 times smaller than the amplitude of the foreshock F_a , and this makes the low-frequency variations invisible in the upper plot.

Figure 3b presents the Yak data in the same 3-h interval. Here, the F_a foreshock amplitudes exceed to a lesser extent the amplitudes of microseisms recorded in a range of periods <1 min (the upper curve). As in the case of the Pet station (Fig. 3a), the foreshock does not distort significantly the structure of variations in the range of periods <1 h (the two lower curves). Maximums at 31 and 13.3 min are recognizable in the periodograms of curves 2 and 3.

Comparison of Figs. 3a and 3b suggests that, during the same time intervals, variations at the Pet and Yak stations differ substantially in their morphological structure and frequency composition, and there are no clear indications that the periodic variations arising at these stations (Fig. 2) are caused by the foreshock F_a .

We applied a similar analysis to a 3-h interval including the foreshock F_b . Figures 4a and 4b show the respective plots for the Pet and Yak stations. As in the preceding case, the foreshock F_b distorts insignificantly the structure of low-frequency variations observed before the shock, particularly in the range of periods exceeding 5 min (the lower curves). Analysis of periodograms revealed maximums at periods of 37.2 and 12.4 min at the Pet station and 23 and 11.5 min at the Yak station. The variations at these two stations differ significantly in their morphology and frequency composition.

The ~ 37 -min period is best resolved at the Pet station (the lower curves in Fig. 4a). Periodic variations at this period were revealed by the $\Delta \ln L$ program in the final hours of the Kronotski earthquake nucleation (the upper diagram in Fig. 2). Note also that, although the amplitudes of the foreshocks F_a and F_b at both of the stations are comparable (Figs. 3a, 3b, 4a, 4b), the periodic variations at the F_a time appeared at both stations but those at the F_b time were present only at the Pet station, located in the Kamchatka seismically active zone (Fig. 2). Variations of the same type continued at the Pet

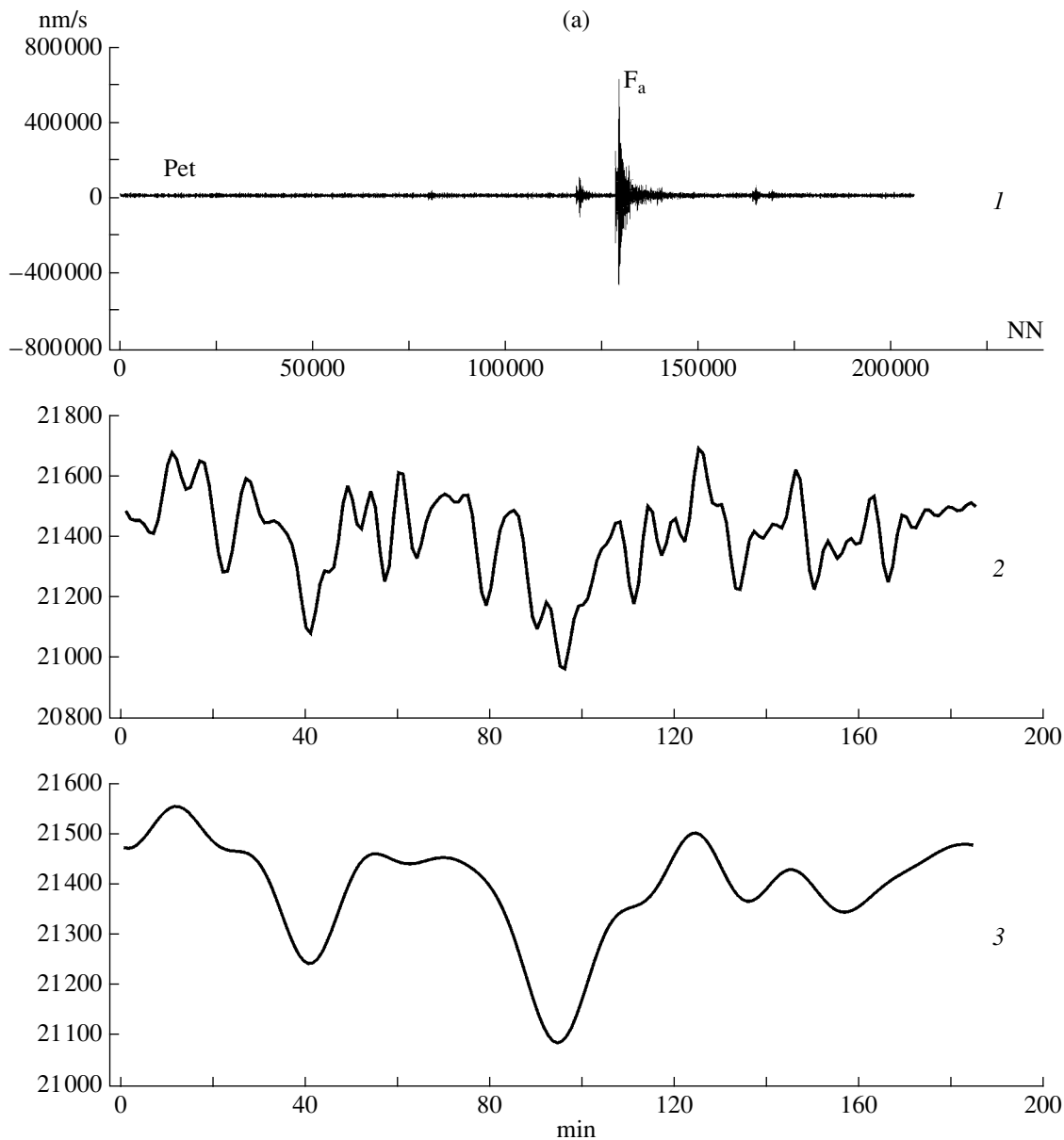


Fig. 3. Records of the Pet (a) and Yak (b) stations including the foreshock F_a : (1) initial records; (2, 3) records obtained after the removal of high frequency variations with periods shorter than (2) 5 and (3) 20 min.

station after the foreshock F_b until the Kronotski earthquake.

We should also note that, as is evident from plot 2 in Fig. 4a, asymmetric pulsed periodic disturbances 37.2 min long are present at the Pet station, whereas they are absent at the Yak station (plot 2, Fig. 4b).

The subsequent analysis is related to the wavelet expansions of the records. In order to compare results for different signals, it is necessary to choose a single basis wavelet. An orthogonal symlet of the 14th order nullifying the first seven moments was found to be an optimal wavelet minimizing the entropy of the distribution of the squared moduli of wavelet coefficients [Mal-

lat, 1998] for the Pet record and was adopted for the subsequent analysis of all signals.

Figure 5a presents the results of the wavelet band-pass filtering of the Pet record after its conversion to 10-s discretization (through averaging and 200-fold thinning of the initial 20 Hz). The first three highest frequency detail levels are removed in the upper plot of Fig. 5a; i.e., only scales no smaller than 160 s are left. In the lower plot of this figure, detail levels of the numbers 4–9, from 160 to 10 240 s (2.84 h), are left. It is noteworthy that these plots contain sequences of nearly regular negative peaks. Below, using the wavelet-packet analysis of this record, we show that these peaks have two characteristic time scales: 22 and 40 min. Such a structure

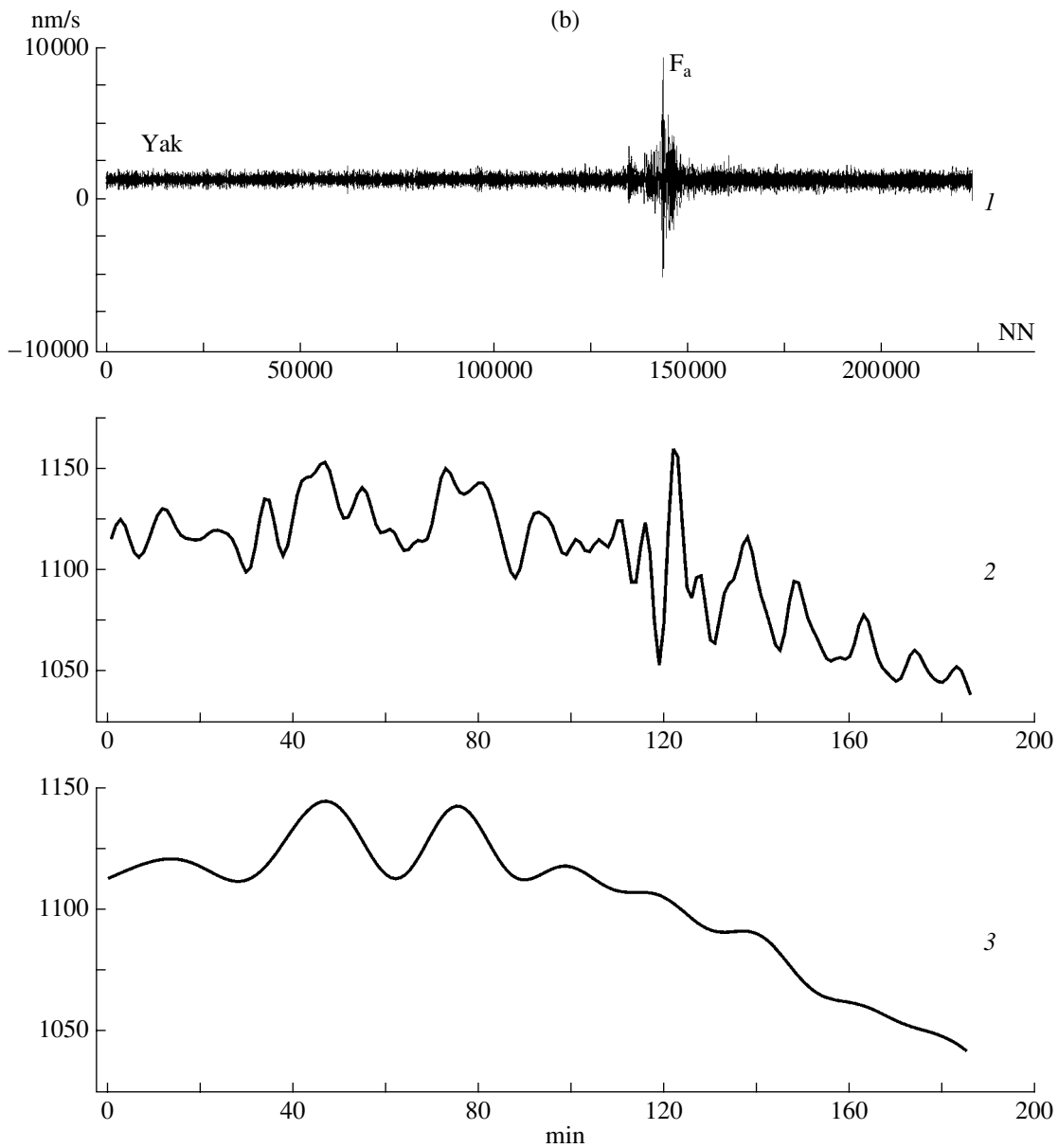


Fig. 3. (Contd.)

is observed in the Pet record alone. For comparison, analogous plots are presented in Fig. 5b for the Yak station: the curves are seen to display chaotic behavior.

Analysis of a longer (compared to the interval of Fig. 5) series of observations showed that the asymmetric variations in the range 30–40 min began at the Pet station on November 30. Three successive intervals of the Pet record in the range of periods from 10 to 100 min are presented in Fig. 6. The time (in hours) is measured from 00:00 UTC of November 20. The vertical bars mark the beginnings of days from November 24 to December 5. It is seen that the variations under consideration arose in the middle of November 30 (~247 h). Analysis of the KEMSP regional catalog

showed that no earthquakes with $K > 8.5$ were recorded in this period, and, according to the ISC catalog, no earthquakes with magnitudes exceeding 5 occurred during this time throughout the world. A preceding earthquake of $K = 9.2$ occurred on Kamchatka 8 h before the onset of variations (242.45 h) and was followed by an earthquake of $K = 8.6$ that occurred 5 h after their onset (255.38 h). Twenty-one earthquakes (≈ 3 events per day) occurred on Kamchatka between the beginning of the period shown in Fig. 6 and the foreshock activation of December 3 before the Kronotski earthquake described above (the arrow F); such seismic activity is typical of this zone. The strongest of these events occurred at 197.95 h ($K = 10.5$), 200.72 h

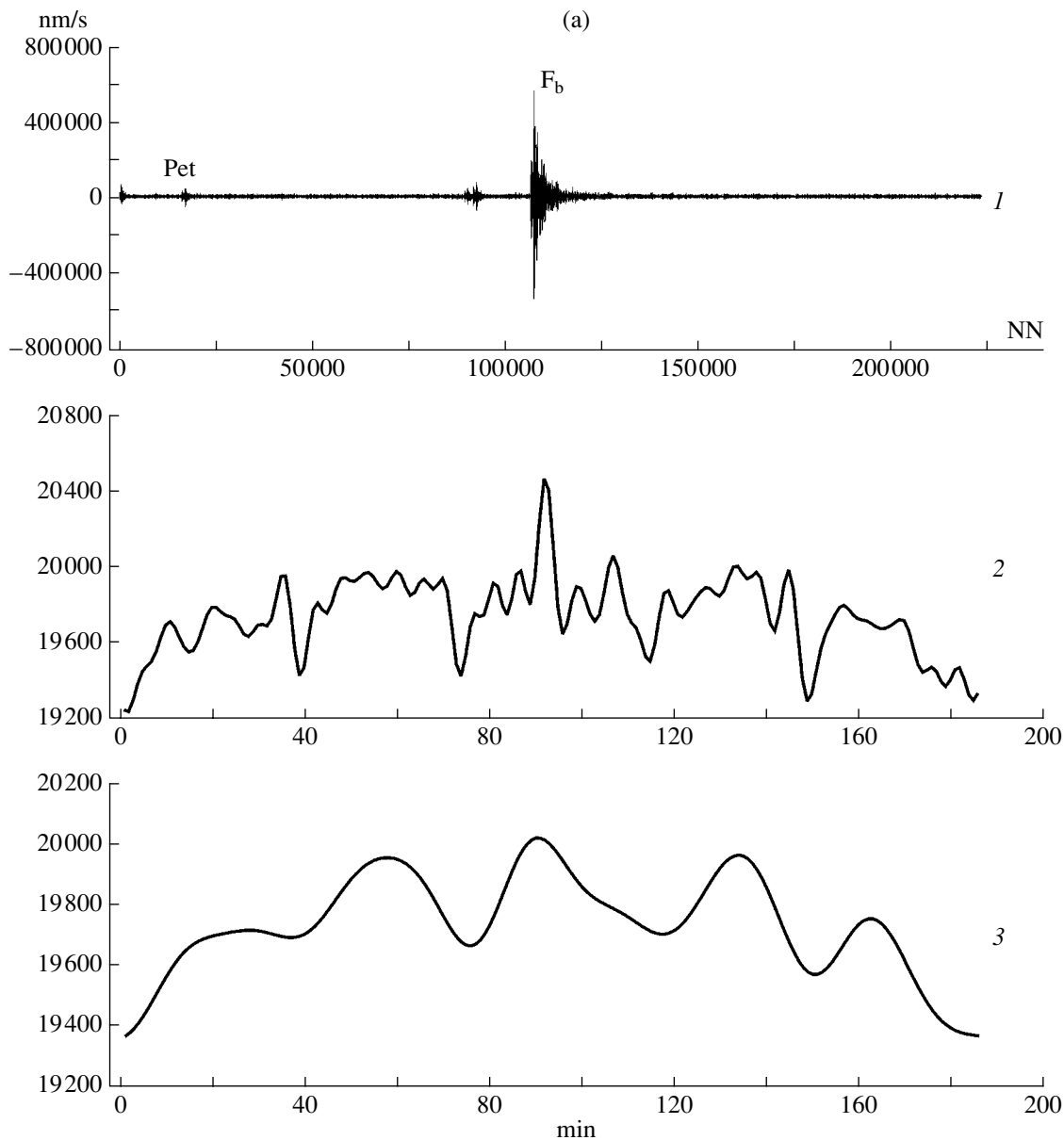


Fig. 4. Records of the Pet (a) and Yak (b) stations including the foreshock F_b : (1) initial records; (2, 3) records obtained after the removal of high frequency variations with periods shorter than (2) 5 and (3) 20 min.

($K = 10.2$), and 269.07 h ($K = 10.3$). No visible features that can be associated with their time moments or with the time moments of the other earthquakes are observed in the plots of Fig. 6.

We also checked whether the time interval of periodic variations detected by the $\Delta \ln L$ program and shown in Fig. 2 can be identified by other, basically different programs of time series analysis.

Figure 7 shows the wavelet expansions at the first nine detail levels (the scale of each plot was chosen automatically) of the seismic records with 10-s discretization intervals for the same five stations and in the same time interval as in Fig. 2. First of all, we should

note that the foreshocks F_a and F_b of the Kronotski earthquake are recognizable at the first three (highest-frequency) detail levels. The lower-frequency detail levels 4–9 contain a series of low-frequency events, but only the event that occurred at about 28.3 h is common to the four stations. This low-frequency event is best resolved at the Yss and Yak stations, less pronounced at the Pet station, and weakest at the Mag station, where only a small burst is noticeable at the eighth detail level (Fig. 7).

The expansion of the Pet record in Fig. 7 is most enriched in low frequency variations. The wavelet-packet diagram (Fig. 8) is useful for its presentation in

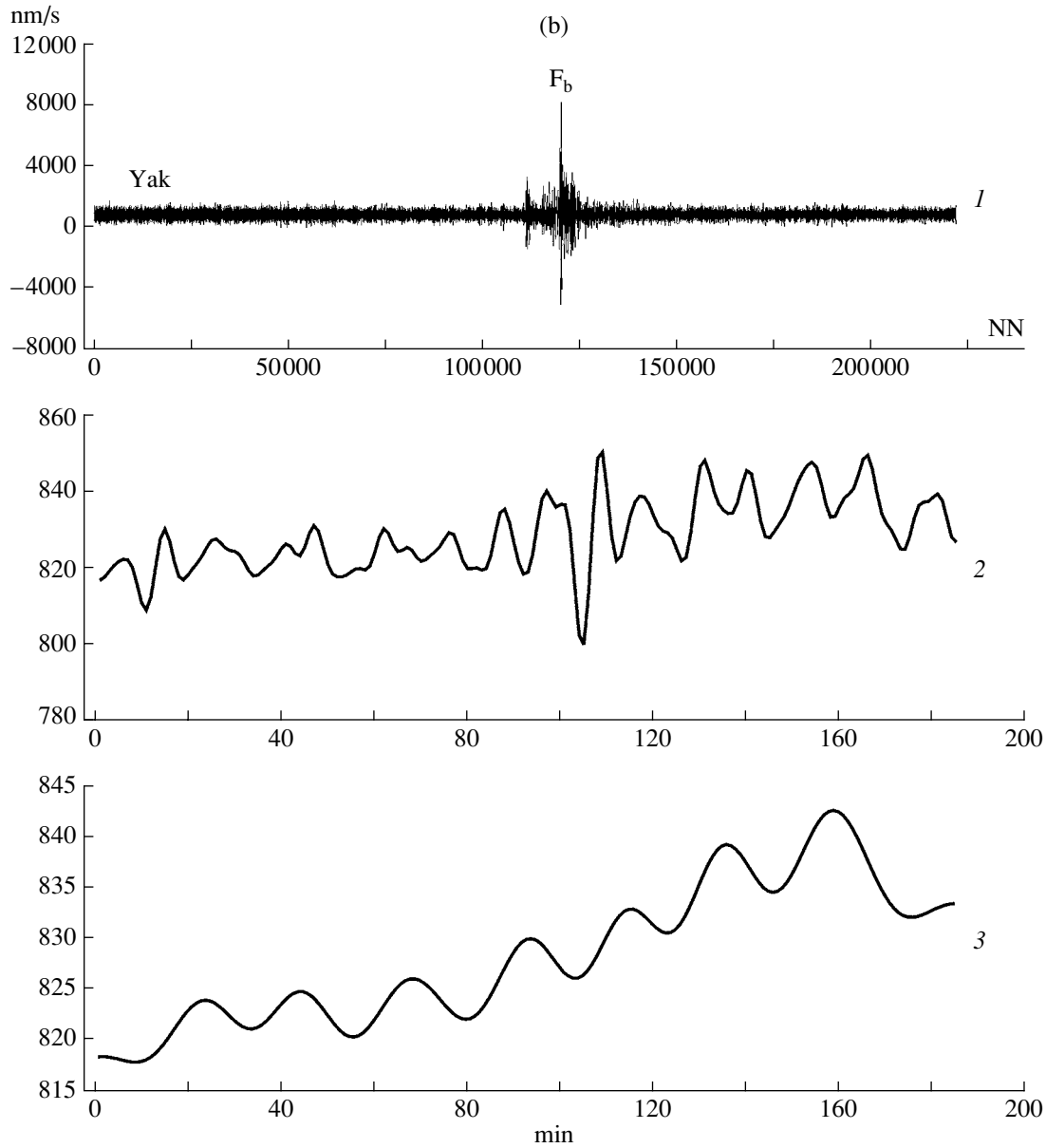


Fig. 4. (Contd.)

greater detail. In this diagram, the detail levels 4–9 are split into eight parts (altogether, 48 frequency bands; these wavelet-packet bands are arranged in ascending order of the common logarithm of the frequency, or scale, central for each band). Two preferred scales are present (two dark bands near logarithmic values of -0.45 and -0.15). These scales were estimated more accurately from the plots of averages of the squared wavelet-packet coefficients in each band (the so-called wavelet-packet spectrum). Two peaks on scales of 22 and 40 min were revealed. Figure 8 shows that the peak at the period 22 min is largely caused by the fluctuation of wavelet-packet coefficient values in this band at about 54 h. The same low-frequency event is clearly

seen in Fig. 7; however, there it is impossible to estimate the energy contribution of each level, which can be done from the analysis of Fig. 8.

Comparison of Fig. 2 with Figs. 7 and 8 shows that, in contrast to the $\Delta \ln L$ program, the wavelet analysis failed to clearly identify the precursory effect in the last interval (80–83 h) before the Kronotski earthquake. This can be attributed to the fact that, from the standpoint of recognition of the effects of synchronization between various processes, wavelet analysis has a substantial drawback: the concept of phase is absent in this approach. Therefore, if peaks are shifted relative to each other by a value exceeding their scale, the wavelet measures of coherence will treat such a situation as the

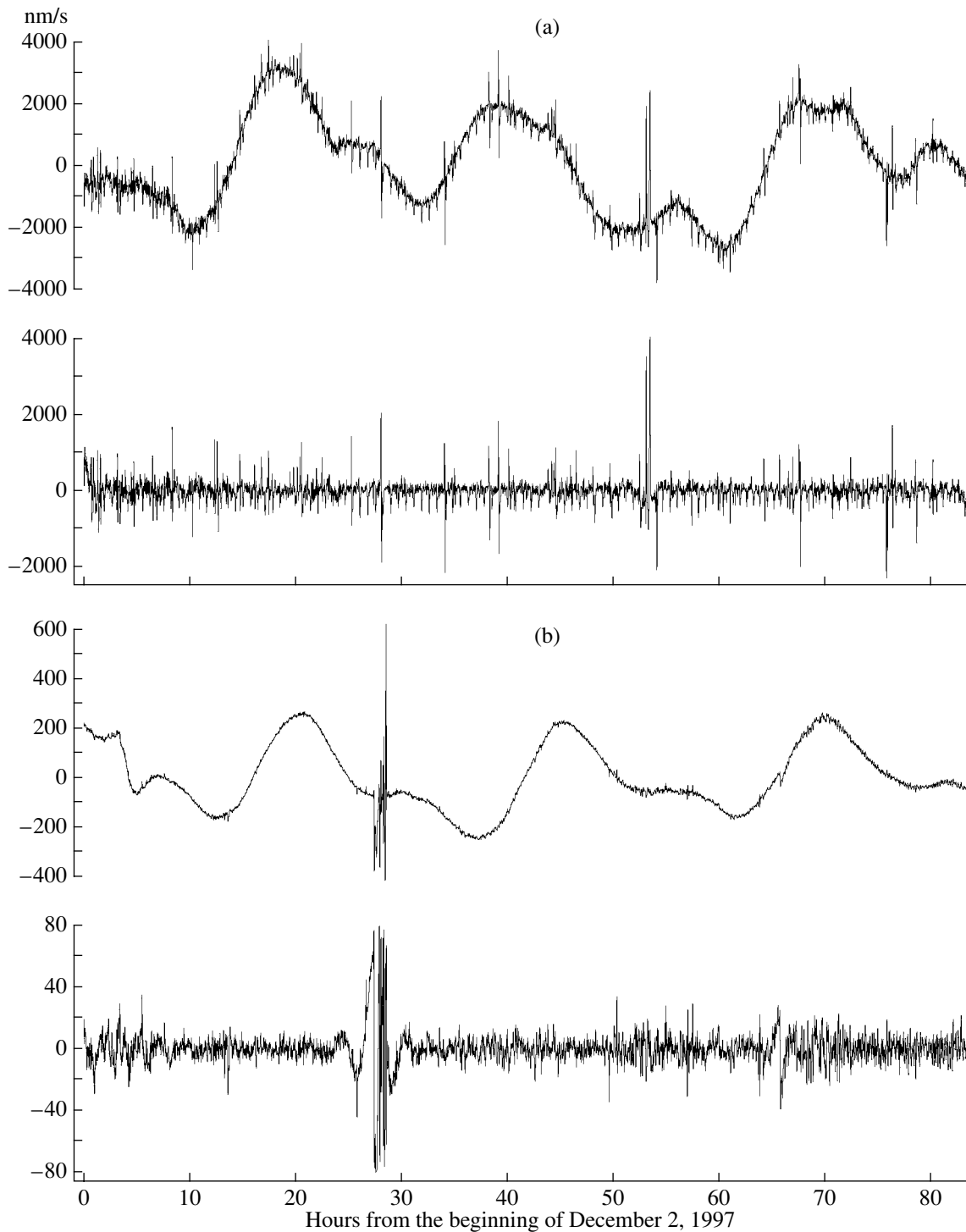


Fig. 5. Results of wavelet filtering of the Pet (a) and Yak (b) records subjected to 10-s discretization. The upper plot in each panel relates to detail levels beginning from the fourth (periods longer than 160 s), and the lower plots relate to detail levels 4–9 (periods from 160 s to 2.84 h).

absence of synchronism. However, pulse-type anomalies that arose, for example, in the interval 30 h and could have been associated with the onset of the foreshock process on Kamchatka were reliably identified by the wavelet analysis.

DISCUSSION

As is evident from Fig. 2, periodic variations are clearly recognizable at four stations (except the Pet station) in the interval 20–30 h and at all five stations in the

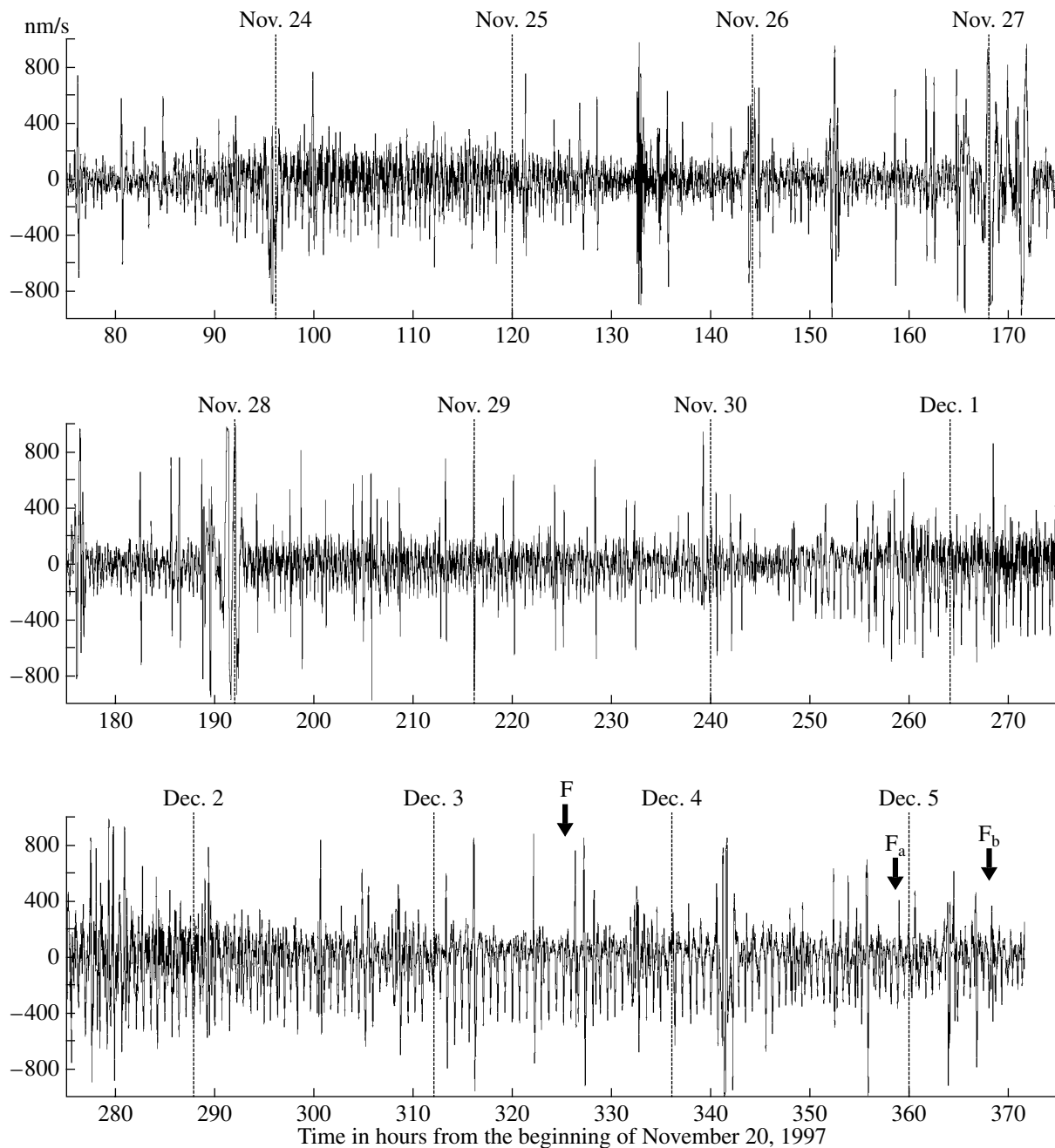


Fig. 6. The low frequency component (periods from 10 to 100 min) of the 30-s discretized Pet record in the interval from November 20, 1997, through December 5, 1997 (strictly up to the time moment of the Kronotski earthquake). The vertical bars mark the beginnings of days, and the arrows mark the time moments of the three strongest foreshocks.

interval 70–80 h. The stations are separated by thousands of kilometers, and their local times differ by 5–9 h; the extrema of earth tides shift by the same time intervals. This indicates that the variations under discussion were not caused by the influence of the Sun or Moon. According to data of meteorological stations, the atmospheric pressure was somewhat lower only near the Mag station (976–984 mbar) and at the other stations varied within 1005–1025 mbar. The wind velocity did not exceed a few meters per second. Note also the pres-

ence of a stable snow cover. Taking into account all these circumstances, we may suggest that a global geodynamic source of unknown nature acted during the time intervals considered. As a response to such a disturbance, the seismic stations recorded periodic variations in microseisms in the range of periods <1 h. Responses recorded by different stations were nonsynchronous, depending on local conditions. In this respect, the Pet station differed most drastically from the other stations: the variations appeared at it 2–5 h

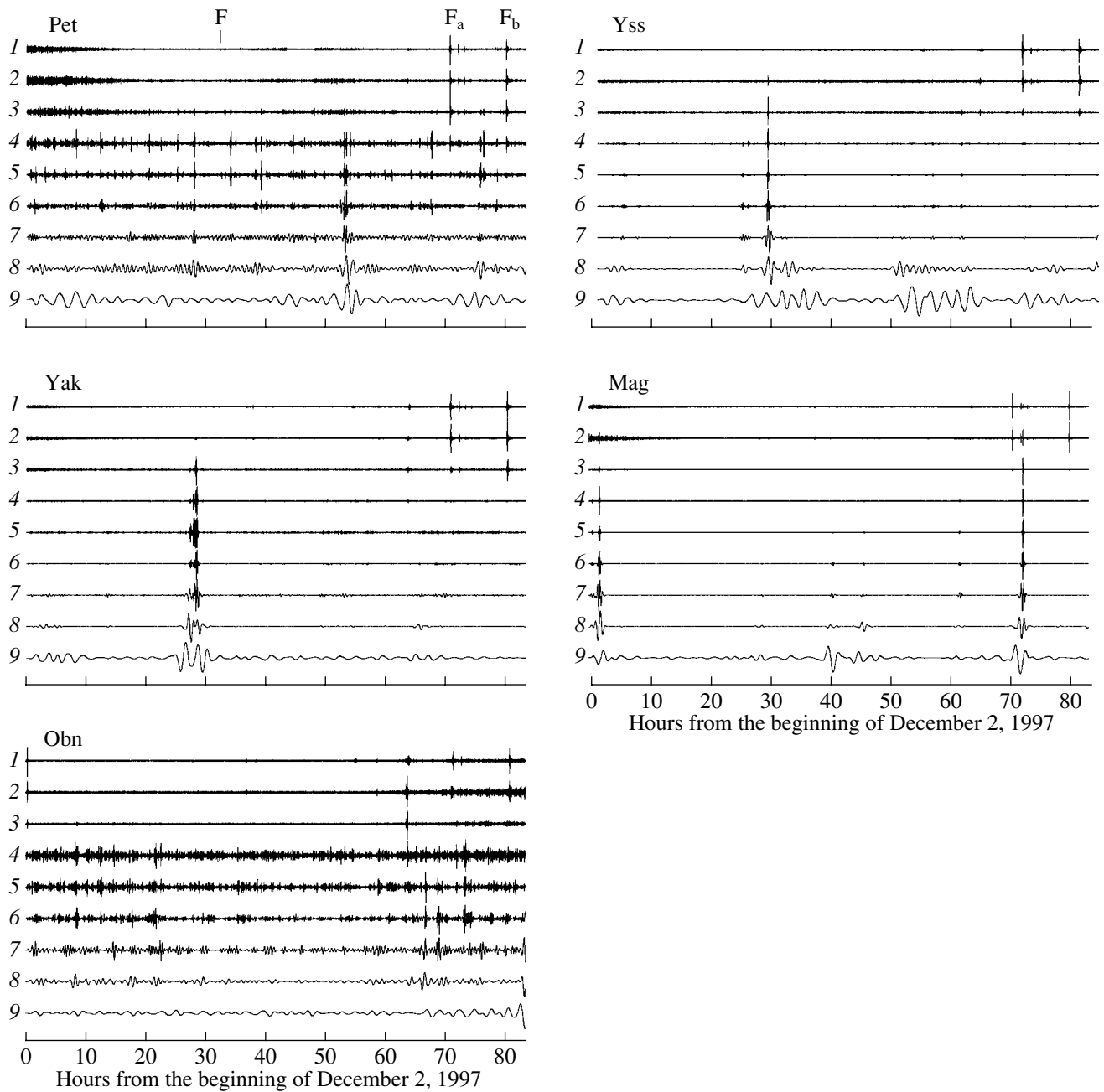


Fig. 7. Wavelet expansions of 10-s discretized seismic records at all five stations for the first nine detail levels.

later than at the other stations, and variations with a period of ~ 37 min observed 3 h before the Kronotski earthquake were recorded by this station alone.

Comparing intervals of periodic variations with the time moments of foreshocks of the Kronotski earthquake (the $\Delta \ln L$ anomalies in Fig. 2), the following facts should be emphasized. Since the anomalies sometimes arose synchronously at widely separated stations, they were not caused by Kamchatka foreshocks. However, the onset of foreshock activation F and the strong foreshocks F_a and F_b were confined to the anomalous

intervals recorded at the Pet station. In our opinion, two plausible conclusions stem from the aforesaid: (1) the occurrence of foreshocks and periodic variation anomalies are two indicators of an unstable state in the lithosphere, and (2) foreshocks can give rise to periodic variations, but the latter can also provoke earthquakes.

The pronounced anomaly in the $\Delta \ln L$ function at the Yss and Yak stations in the interval 28–31 h and the absence of this anomaly at the Pet station during the same interval are apparently due to the following factors. Plots of initial realizations at a sampling frequency

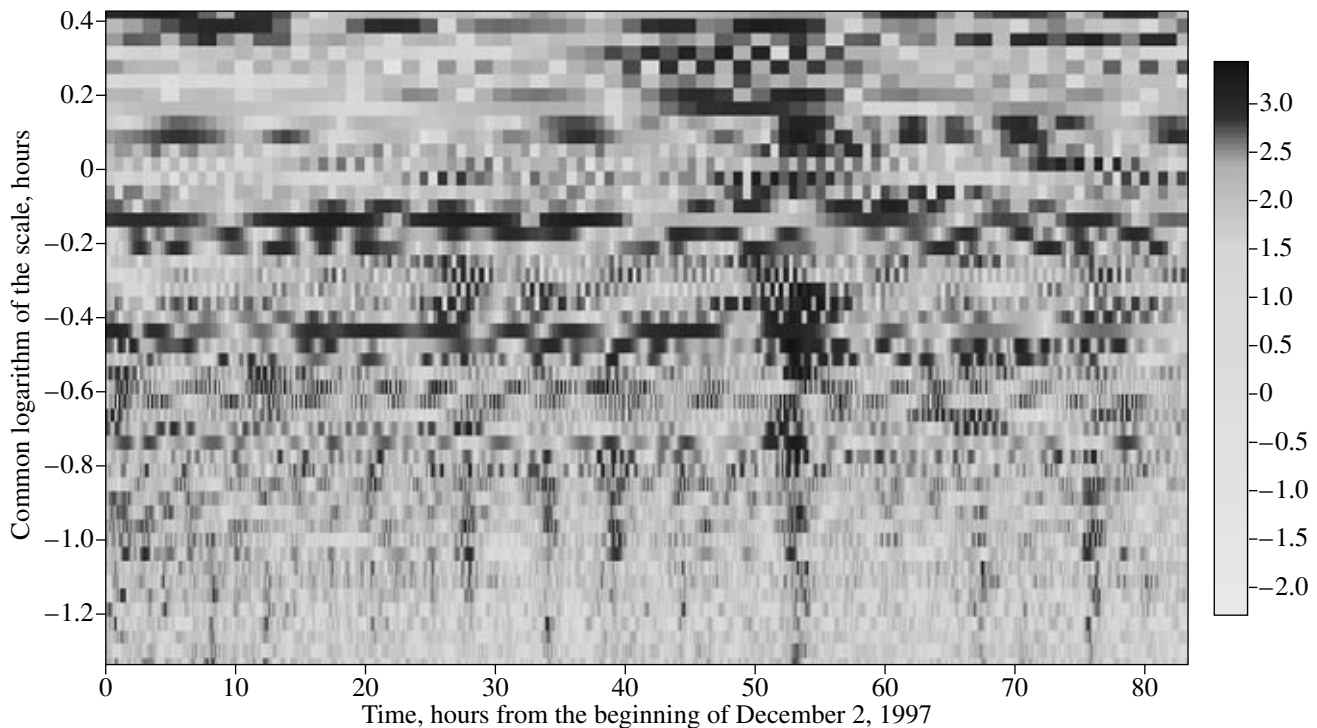


Fig. 8. Diagram of the modified wavelet-packet coefficients of the expansion of the 10-s discretized Pet record for the detail levels 4–9.

of 20 Hz recorded at the above stations are presented in Fig. 9. The plots begin from 04:00 UTC of December 3, which corresponds to 28 h in Fig. 2. A disturbance in the form of a unipolar pulse about 3 min long was recorded at the Yss station at 04:25 UTC. A disturbance of a more complex shape was recorded at the Yak station in the same time interval. No anomalous disturbances exceeding the level of microseisms were recorded at the Pet station. No earthquakes in the time interval under discussion are noted in the ISC world seismic catalog and in the regional catalogs of Kamchatka and Sakhalin published by the RAS Geophysical Service. According to data of the meteorological stations located near the Yss, Yak, Mag, and Pet stations, no anomalous meteorological phenomena were noted either. In this connection, it may be suggested that, at 04:25 UTC on December 3, 1997, a geodynamic movement occurred beneath the Sea of Okhotsk. The shape of the unipolar pulse recorded at the Yss station apparently indicates that its source was located within the wavelength. The question of whether the fact that the intense foreshock activity preceding the Kronotski earthquake started 5 h after this event is accidental or there is a physical relation between these phenomena remains open. However, the space–time correlations between the Sea of Okhotsk and Kamchatka earthquakes have been noted in a number of works [Sobolev, 1994; Zakharova and Rogozhin, 2004]. Information based only on seismic variations is insufficient for confirming or disproving the geodynamic nature of an

anomaly. Unfortunately, we failed to find any data on crustal deformations in the region under investigation in the time interval considered.

Comparison of Figs. 5–7 with Fig. 2 shows that pulsed variations were observed in fairly long intervals; however, only in rare cases did they cause anomalies in $\Delta \ln L$, i.e., they were periodic. This implies the presence of a mechanism of synchronization by a lithospheric or external source, and such a synchronization is not necessarily associated with an increase in the amplitude of variations. According to a rather widespread point of view [Pykovsky *et al.*, 2003; Chelidze and Matcharashvili, 2003], synchronization arises in a medium that is in the state of unstable equilibrium and is characterized in this case by an increased sensitivity to external effects. In our case, the synchronization manifested itself not only on Kamchatka (the Pet station), which was apparently in a metastable state before the Kronotski earthquake. This indicates that synchronization effects arise in various, including seismically passive, regions of the lithosphere. Consequently, either these effects are caused by an internal self-organization of the geodynamic process or vast regions of the lithosphere are highly sensitive to strain.

Nonlinear wavelet filtering with the use of the Donoho–Johnstone threshold [Donoho and Johnstone, 1994; Mallat, 1998] was additionally applied in order to compare Fig. 2 with the results of wavelet analysis. To accomplish this procedure, the coefficients after the wavelet transform are arranged in increasing order of

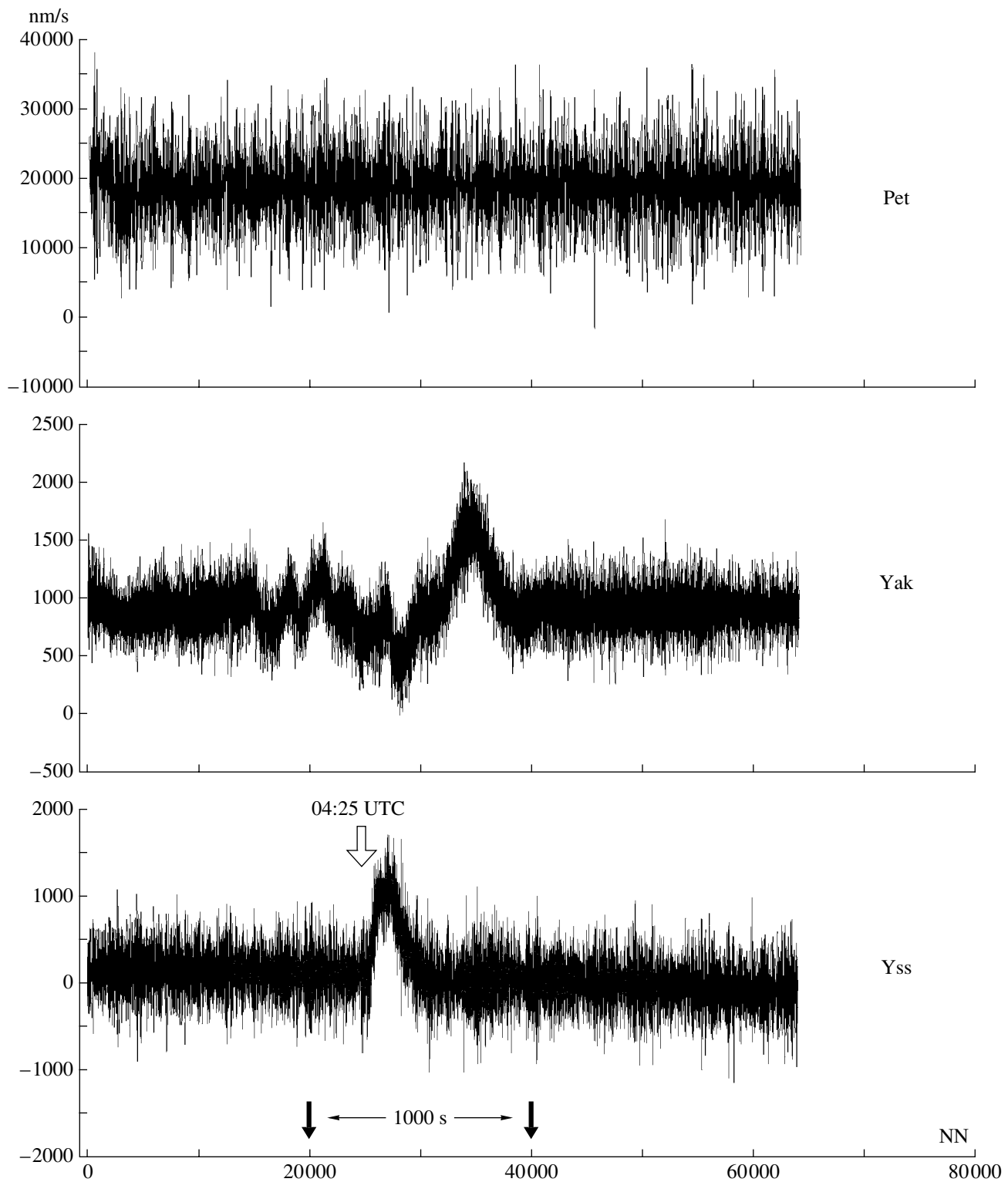


Fig. 9. Records of the Pet, Yak, and Yss stations in the period when a low-frequency pulse (supposedly of geodynamic origin) appeared at the Yak station; the NN values are the numbers of 20-Hz discretized discretization points.

their absolute values and are then divided into “large” and “small” values, regardless of the detail level to which they belong. The essence of the method consists

in a substantiated choice of the threshold value separating large and small coefficients. The inverse transformation with the large coefficients yields the most infor-

mative and compact signal, and all the rest is regarded as “noise.” This method with some modifications was used in [Lyubushin *et al.*, 2004] for automatic classification of three-component seismic records. In the case of the records with 30-s discretization intervals analyzed for the first seven detail levels, the “large” values account for 1–2% of the total number of coefficients in the range from 1 to 128 min. The informative and noisy signals revealed by such a procedure are presented in Fig. 10 for each station as the upper and lower plots, respectively. The nonstationarity observed in the lower plots (noisy components) is obviously nondiurnal.

Comparing Fig. 10 with Fig. 2, we see that pulses in the informative signals occasionally coincide in time with the anomalies of the periodic variations $\Delta \ln L$ (intervals of 28–31 and 71–75 h). However, this is not the case, for example, for the time interval between the foreshock F_b and the Kronotski earthquake. On the contrary, some intervals of informative pulses in Fig. 10 (50–54 h at the Pet station, 50–60 h at the Yss station, and 40–47 h at the Mag station) are unrecognizable in the $\Delta \ln L$ anomalies in Fig. 2. Thus, the occurrence of the foreshocks and the Kronotski earthquake is unrelated to the informative pulses of microseismic variations. The same follows from our analysis of the noise level at the five stations under consideration.

If we consider the periods from 8 to 128 min (Fig. 11), the noises are nonstationary, and the period ~ 40 min, observable in Figs. 5 and 6, is also identified at the Pet station. Figure 11 shows that, during the analyzed time interval, no significant changes in the noise level were noted at any of the five stations for the four days before the Kronotski earthquake. The same is valid for the last interval (3 h before the earthquake), when a well-expressed precursor arose as a $\Delta \ln L$ maximum (Fig. 2). Figure 11 can also be used for comparing noise levels at different stations taking into account the calibration data kindly provided by the RAS Geophysical Service. The IRIS stations ensure the calibrated reception of signals within the range 5–0.0028 Hz [Starovoit and Mishatkin, 2001] (the lower limit corresponds to a period of 6 min). We examined the level of microseisms in the range from 1 s to 30 min at all five stations under consideration, as well as at the Arti station in the Ural region, and found that the microseisms have maximum amplitudes in the range 3–5 s, which agrees with the model of their oceanic origin. As the period becomes longer, the amplitudes decrease, dropping on average by a factor of 20 at the 1-min period. Then the amplitude decrease slows down, and the amplitudes start gradually rising after a period of 5–10 min. Qualitatively, the power spectra of the variations are similar to the spectrum for the Pet station, shown in Fig. 1. However, the larger the distance from the Pet station, the slower the amplitude drop with increasing periods in the range from seconds to a few minutes. Thus, the variation rates plotted as ordinates in Fig. 11 allow us to draw the following preliminary con-

clusion: their gradual decrease with increasing distance from Kamchatka (the Pet station) and their level at the Pet station, which is an order of magnitude higher than at the other stations, imply that the source of these variations is located in the Pacific seismically active zone. A comprehensive investigation of the level and variability of microseisms recorded by broadband stations is outside the scope of this work but seems to be of primary interest from the standpoint of understanding the Earth’s “breathing.”

Calculations of the $\Delta \ln L$ function from data of the Kamchatka seismic catalog and laboratory modeling showed that precursors in the form of hidden periodic variations preceding an earthquake or fracture of a sample typically have a period gradually increasing as a catastrophe approaches [Sobolev, 2003]. In the paper [Sobolev, 2004], devoted to the analysis of a precursor of the Kronotski earthquake in the 10–100-min range of microseismic variations, this feature was somewhat indistinctly expressed, apparently due to substantial averaging of the spectral peaks identified by the $\Delta \ln L$ program. In this connection, we calculated the spectral time analysis diagram of the common logarithm of the power spectrum from data recorded at the Pet station before the Kronotski earthquake. This diagram, shown in Fig. 12, was obtained for a low frequency noisy signal after its 30-s discretization and the removal of informative pulses by the threshold filtering, i.e., for the signal presented in Fig. 11 (Pet) in the range of periods from 10 to 100 min.

Figure 12 shows that, as the moving window (4 h wide) approaches the time moment of the Kronotski earthquake, the frequency of the main rhythm progressively decreases, with its period changing from 25 to 40–50 min. Thus, the evolution of the spectrum from short toward longer periods noted in [Sobolev, 2003, 2004] is confirmed.

Calculations of microseismic variations (with the use of the programs described above) from data recorded at the Pet station during one day after the Kronotski earthquake revealed that the low frequency components with periods exceeding 10 min were no longer present. This additionally indicates that they were induced by the earthquake nucleation process.

We do not know studies other than [Sobolev, 2004] that have reported periodic variations in microseisms arising several hours before a strong earthquake. The most similar results appear to have been obtained in [Petrova, 2002; Levin and Sasorova, 1999]. In the first of these papers, seismogravitational variations in a range of periods of 1–5 h recorded at GEOSCOPE stations were investigated. Petrova noted: “The absence of any substantial differences between the oscillation spectra calculated from records before and after strong earthquakes indicates that seismogravitational oscillations are independent of the Earth’s seismicity. Presumably, these oscillations are related to deformation pro-

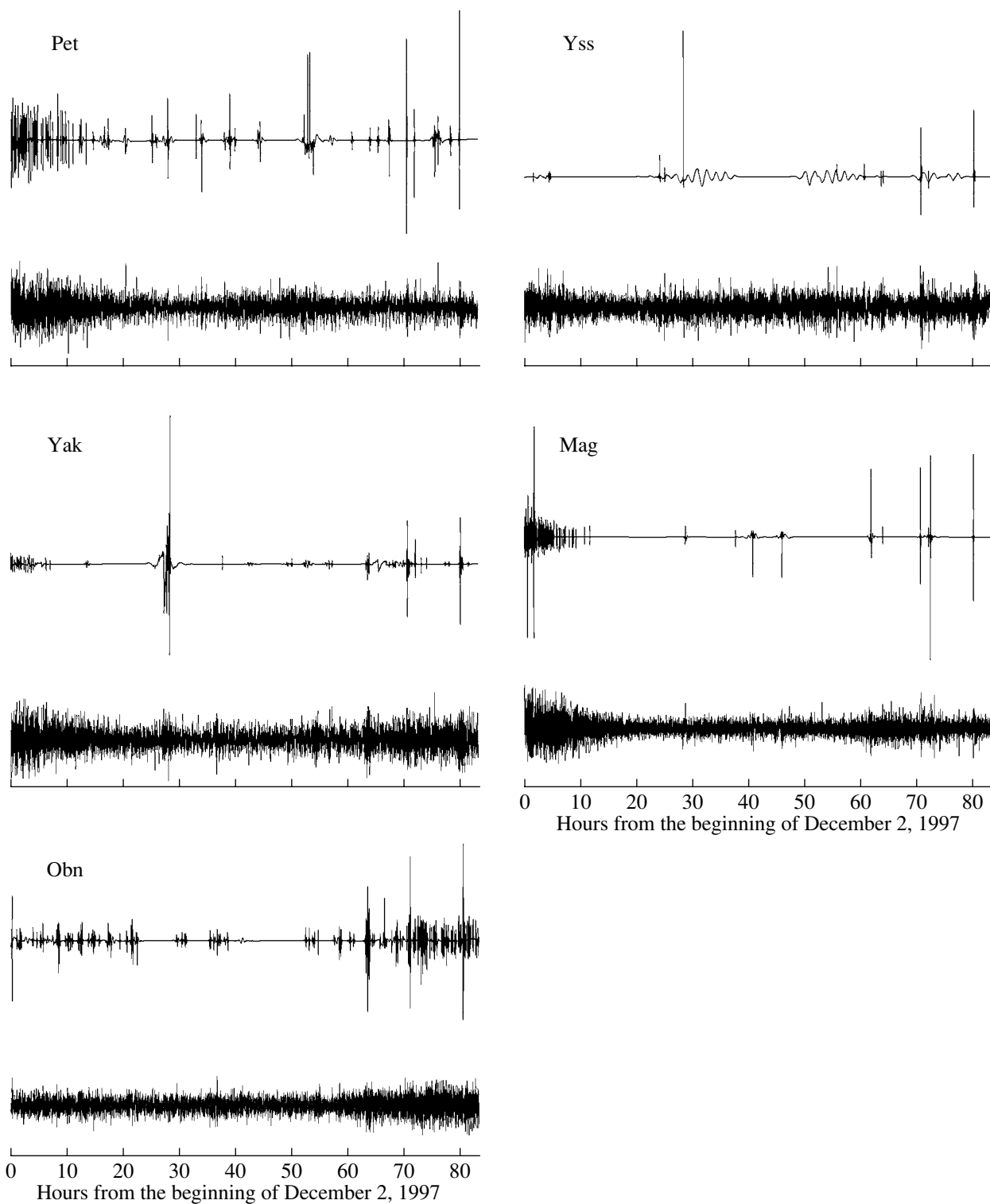


Fig. 10. The results of the Donoho–Johnstone threshold filtering of 30-s discretized seismic records at the five stations for the detail levels 1–7. For each station, the upper plot in each panel shows the most informative variations in the signal and the lower plots show noisy variations.

cesses, in particular, within the continent with a complex hierarchical block structure.”

Levin and Sasorova [1999] established that “low frequency premonitory signals” with periods of 3 to

200 s preceding the arrival of the *P* wave at the Yuzhno-Sakhalinsk IRIS station from some earthquakes of the Kurile–Kamchatka zone are present in seismograms in the interval from a few seconds to 1.5 h. Taking into consideration recorded data on “slow earthquakes” in

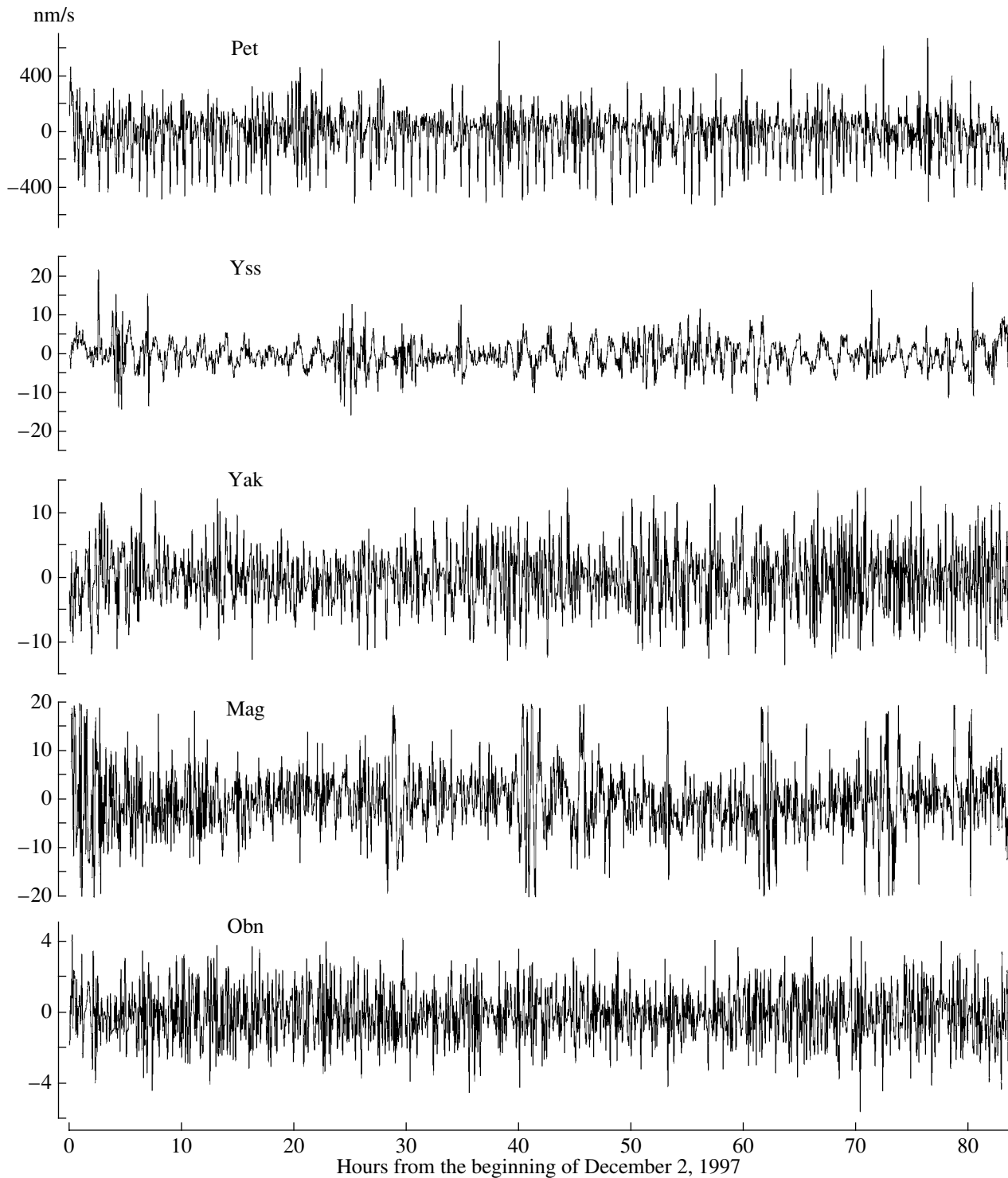


Fig. 11. Noisy components of 30-s discretized seismic records at the five stations after threshold filtering and removal of the first three detail levels (the resulting range of periods is 8–128 min).

various seismically active regions of the world, Levin and Sasorova derived the following relation between the period of these variations T and the size of their source L :

$$T = B \cdot L^{1/2}, \quad (23)$$

where the coefficient B is equal to $0.02 \text{ s/cm}^{1/2}$. According to (23), the linear size of a radiator of such variations must not exceed a few tens of kilometers, which is comparable with the dimensions of earthquake sources.

Formula (23) is unlikely to be applicable to the microseismic variations with a period of ~ 40 min that

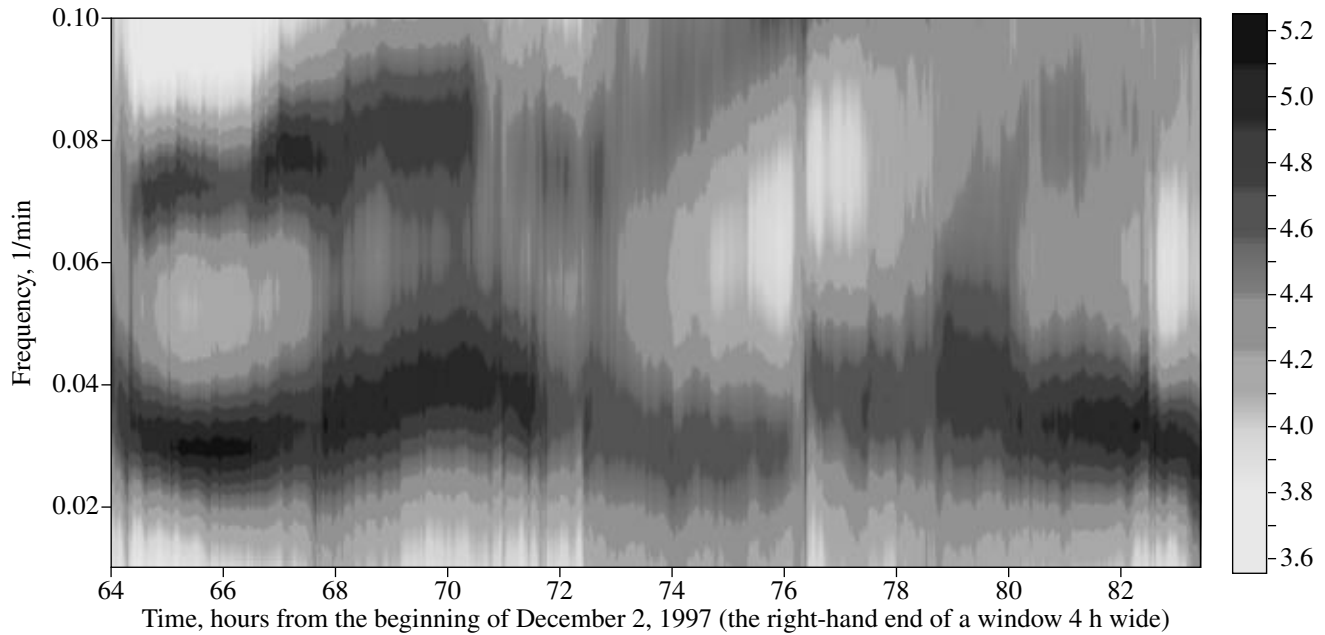


Fig. 12. Evolution of the common logarithm of the power spectrum of low frequency noise at the Pet station (Fig. 11) estimated with a moving window 4 h wide (480 values of the 30-s discretized record). The maximum-entropy method was applied with an AR order of 40 and a period range of 10–100 min.

are discussed in this work because the source size in this case should exceed the Earth's radius by a few orders of magnitude. Of course, this does not imply that the origin of the microseismic variations is unrelated to the source of a forthcoming earthquake. For example, we cannot rule out the following mechanism: very weak variations in the gravitational field (overtones of free oscillations of the Earth or wave motions in the asthenosphere) permanently act on an earthquake source, but their amplitude starts rising nonlinearly only when this source reaches a metastable state due to an increase in the strain sensitivity of the medium. To elucidate the nature of the phenomenon recorded, microseismic data need to be complemented by results of investigation of other geophysical fields.

CONCLUSIONS

The following main results have been obtained from the study of synchronous records of microseisms in the range of periods <1 h obtained at the Petropavlovsk, Yuzhno-Sakhalinsk, Magadan, Yakutsk, and Obninsk stations with the use of various programs of processing and analysis of time series.

The predominant variation periods and their number vary in time in records of each station and are different at different stations.

There exist stability intervals for one or several periods (synchronization intervals), giving rise to maximums in their spectrum. These intervals can either coincide or not coincide in time at different stations. No

anomalous meteorological effects were recorded during these time intervals.

The self-organization of the seismic process or a selective response of the medium to weak effects of cosmic, meteorological, or intraterrestrial origin can be responsible for the synchronization intervals. The time and intensity of their manifestation depend on global and regional geodynamic factors.

Synchronization intervals at the Pet station include the Kamchatka strongest foreshocks of the Kronotski earthquake; i.e., the probability of earthquake occurrence increases during such periods.

The Pet record differs from records of the other stations in that it includes asymmetric variations of the relaxation type preceding the Kronotski earthquake. These variations arose five days before the earthquake and three days before the onset of intense foreshock activation. The amplitude of periodic variations recorded at the Pet station is an order of magnitude higher compared to the other stations, implying that the source of these variations is located in the Pacific seismically active region.

The number of predominant periods at the Pet station decreases toward the time moment of the Kronotski earthquake, so that the polymodal spectrum of the variations is transformed into a unimodal one. Shorter periods disappear, and a period of 37 min becomes predominant 1 h before the earthquake.

The synchronization intervals of variations, as well as the foreshock activation, are indicators of an unstable state of a seismically active region.

ACKNOWLEDGMENTS

This work was performed within the framework of the program "Electronic Earth" of the Presidium of the Russian Academy of Sciences and was supported by the program "Leading Scientific Schools," project no. NSh-1270.2003.5.

REFERENCES

1. S. Aoki, M. Ohtake, and H. Sato, "Tidal Modulation of Seismicity: An Indicator of the Stress State?" in *The 29th IASPEI General Assembly, August 18–28, 1997. Thessaloniki, Greece. Abstracts*, p. 347.
2. P. Bak, S. Tang, and K. Winsensfeld, "Earthquakes as Self-Organized Critical Phenomenon," *J. Geophys. Res.* **94**, 15 635–15 637 (1989).
3. T. Chelidze and T. Matcharashvili, "Electromagnetic Control of Earthquake Dynamics?" *Comput. Geosci.* **29**, 587–593 (2003).
4. C. K. Chui, *An Introduction to Wavelets* (Academic, San Diego, 1992).
5. D. R. Cox and R. A. W. Lewis, *The Statistical Analysis of Series of Events* (Methuen, London, 1966).
6. I. Daubechies, *Ten Lectures on Wavelets* (SIAM, Philadelphia, 1992).
7. P. G. Djadkov, "Induced Seismicity at the Lake Baikal: Principal Role of Load Rate," in *The 29th General Assembly, August 18–28, 1997. Thessaloniki, Greece. Abstracts*, p. 359.
8. D. Donoho and I. Johnstone, "Ideal Spatial Adaptation via Wavelet Shrinkage," *Biometrika* **81**, 425–455 (1994).
9. B. V. Levin and E. V. Sasorova, "Low Frequency Seismic Signals as Regional Indicators of Earthquake Nucleation," *Vulkanol. Seismol.*, No. 4, 108–115 (1999).
10. A. A. Lyubushin, Jr., "Periodicities and Rhythms of Global Seismicity in the 20th Century," in *Joint Session of the OGGGN RAN Seminar "Theoretical Problems of Geology" and the 10th Seminar "Planetary System of the Earth": Rhythms and Cycles in Geology as Evidence for General Laws of Development. February 7–8, 2002. Abstracts* (OGGGN RAN, Moscow, 2002) [in Russian].
11. A. A. Lyubushin, Jr., V. F. Pisarenko, V. V. Ruzhich, and V. Yu. Buddo, "Identification of Periodicities in the Seismic Regime," *Vulkanol. Seismol.*, No. 1, 62–76 (1998).
12. A. A. Lyubushin, Jr., Z. Kalab, and N. Chastova, "Application of Wavelet Analysis to the Automatic Classification of Three-Component Seismic Records," *Fiz. Zemli*, No. 7, 50–56 (2004) [*Izvestiya, Phys. Solid Earth* **40**, 587–593 (2004)].
13. S. Mallat, *A Wavelet Tour of Signal Processing* (Academic, San Diego, 1998).
14. A. V. Nikolaev and V. A. Nikolaev, *Earth Tides Triggering of Continental Earthquakes* (Seismological Press, Beijing, 1993), pp. 319–327.
15. L. N. Petrova, "Seismogravitational Oscillations of the Earth from Observations by Spaced Vertical Pendulums in Eurasia," *Fiz. Zemli*, No. 4, 83–95 (2002) [*Izvestiya, Phys. Solid Earth* **38**, 325–336 (2002)].
16. W. H. Press, B. P. Flannery, S. A. Teukolsky, and W. T. Vetterling, *Numerical Recipes*, 2nd ed. (Univ. Press, Cambridge, Cambridge, 1996), Chap. 13.
17. A. Pykovsky *et al.*, *Synchronization. A Universal Concept in Nonlinear Science* (Univ. Press, Cambridge, 2003).
18. B. G. Rulev, "Annual Periodicity in the Emission of Microearthquakes and the Irregularity of the Earth's Rotation," in *Earthquakes and Processes of Their Nucleation* (Nauka, Moscow, 1991), pp. 127–138 [in Russian].
19. L. N. Rykunov, O. B. Khavroshkin, and V. V. Tsyplakov, "Lunisolar Tidal Periodicity in Spectral Lines of Temporal Variations in High Frequency Microseisms," *Dokl. Akad. Nauk SSSR* **252** (3), 577–580 (1980).
20. M. A. Sadovsky, *Multidisciplinary Studies of Earthquake Physics* (Nauka, Moscow, 1989), pp. 3–8 [in Russian].
21. V. A. Saltykov, V. I. Sinitsyn, and V. N. Chebrov, "Study of High Frequency Seismic Noise from Data of Systematic Observations in the Kamchatka Region," *Fiz. Zemli*, No. 3, 39–47 (1997).
22. G. A. Sobolev, "On the Relation between Strong Earthquakes of the Kurile–Kamchatka Zone," in *Federal System of Seismological Observations and Earthquake Prediction. Information and Analysis Bulletin* (MChS–RAN, 1994), pp. 68–70 [in Russian].
23. G. A. Sobolev, "Evolution of Periodic Variations in the Seismic Intensity before Strong Earthquakes," *Fiz. Zemli*, No. 11, 3–15 (2003) [*Izvestiya, Phys. Solid Earth* **39**, 873–884 (2003)].
24. G. A. Sobolev, "Microseismic Variations Prior to a Strong Earthquake," *Fiz. Zemli*, No. 6, 3–13 (2004) [*Izvestiya, Phys. Solid Earth* **40**, 455–464 (2004)].
25. D. Sornette and C. G. Sammis, "Complex Critical Exponents from Renormalization Group Theory of Earthquakes: Implications for Earthquake Predictions," *J. Phys. Inst. France* **5**, 607–619 (1995).
26. O. E. Starovoit and V. N. Mishatkin, *Seismic Stations of the Russian Academy of Sciences* (Geofiz. Sluzhba RAN, Moscow, 2001) [in Russian].
27. A. D. Sytinskii, "Solar Activity Implications for Recent Tectonic Movements," *Geomagn. Aeron.* **3** (1), 148–156 (1963).
28. Yu. S. Tyupkin, "Modulation of Weak Seismicity by Tidal Deformations before Strong Earthquakes," *Vulkanol. Seismol.*, No. 3, 3–10 (2002).
29. A. I. Zakharova and E. A. Rogozhin, "Spatiotemporal Relations between Sources of Strong Earthquakes and Their Deep-Seated Precursors," in *Geophysical Investigations* (OIFZ RAN, Moscow, 2004), pp. 13–20 [in Russian].
30. V. N. Zharkov and V. P. Trubitsyn, *Physics of Planetary Interiors* (Nauka, Moscow, 1980) [in Russian].